minerals

MDPI

Review

Mineralogy-Guided Processing of Mining and Metallurgical Wastes into Geopolymeric and Alkali-Activated Materials

Aigerim Imash [1,2], Gaukhar Smagulova [1,*], Vladimir Efremov [1], Kaster Kamunur [1,2], Lyazzat Mussapyrova [1,2], Aisulu Batkal [1,2], Ryskul Azhigulova [2], Aisulu Zhussupova [2] and Anton Kononov [1]

[1] Institute of Combustion Problems, 172 Bogenbay Batyr Str., Almaty 050012, Kazakhstan; iimash.aigerim@gmail.com (A.I.); vlaefremov@mail.ru (V.E.); kamunur.k@mail.ru (K.K.); lyazzat.mussapyrova@gmail.com (L.M.); abatkalova@mail.ru (A.B.); konan_hitech@mail.ru (A.K.)

[2] Faculty of Chemistry and Chemical Technology, Al-Farabi Kazakh National University, 71 Al-Farabi Ave., Almaty 050040, Kazakhstan; azhigulova.ryskul@kaznu.kz (R.A.); zh.aisulu@mail.ru (A.Z.)

* Correspondence: smagulova.gaukhar@gmail.com

Abstract

Mining and metallurgical wastes contain potentially valuable mineral resources but pose growing environmental risks. This review proposes a mineralogy-guided framework for converting these wastes into low-carbon binders and construction materials. Rather than classifying residues by origin or bulk oxide composition, it distinguishes them according to the reaction roles of their mineral phases. The framework first distinguishes self-sufficient systems, in which activation unlocks the intrinsic mineral inventory of the waste sufficiently for matrix or product formation, from mineralogically compensated systems, in which additional functional mineral solids are required to supply deficient reactive Si, Al, Ca, sulfate, alkalinity, or other phase-forming components. Binary and multicomponent formulations are then interpreted according to the specific mineralogical functions supplied by the complementary solids and the resulting changes in reaction pathways and products. Thermal, hydrothermal, mechanochemical, alkaline, and carbonation-based processing routes are compared in relation to phase composition, co-precursor function, and the mechanical, thermal, and service properties of concretes, foams, and backfill materials. Evidence indicates that performance depends more on chemical complementarity than on maximizing waste content. Environmental benefits must also account for contaminant immobilization, carbon dioxide binding, and the energy and reagent demand of pretreatment. Mineralogy-informed machine-learning models may support inverse mixture design, but their transferability remains constrained by feedstock heterogeneity and limited standardized data. The framework links mineralogy, processing, reaction products, performance, and scale-up.

Keywords: precursor mineralogy; mine tailings; metallurgical slags; red mud (bauxite residue); alkali-activated materials; geopolymers; mine backfill; machine learning

Check for updates

Academic Editor: João Castro-Gomes

Received: 12 August 2026
Revised: 7 September 2026
Accepted: 10 September 2026
Published: 13 September 2026

Copyright: © 2026 by the authors. Licensee MDPI, Basel, Switzerland. This article is an open access article distributed under the terms and conditions of the Creative Commons Attribution (CC BY) license.

1. Introduction

The large-scale generation of mining and metallurgical wastes has made their long-term storage a dual challenge: It entails the loss of potentially valuable mineral resources while posing serious environmental and geotechnical risks [1–3]. Available statistics reinforce these concerns: More than 5 billion tonnes of mine tailings are generated annually, while the copper industry alone produces approximately 25 million tonnes of slag per year [4,5]. These wastes, however, are not chemically homogeneous bulk materials. Their

mineralogical composition varies with ore type and processing history and may include quartz, feldspars, glassy silicates, iron and aluminium oxides and hydroxides, sulfides, carbonates, sulfates, and residual alkalis [6–8]. Consequently, their environmental safety and suitability for secondary use are governed less by bulk oxide contents than by phase assemblage, crystallinity, particle-size distribution, and element speciation. The convergence of environmental and resource constraints—the need to utilize accumulated wastes and the drive to decarbonize construction materials—therefore makes the development of alternative binders from mineral residues an important pathway within the circular economy. One of the most promising approaches is the production of geopolymers and alkali-activated materials (AAMs) from aluminosilicate wastes. These materials can incorporate high fractions of secondary raw materials, and substantial reductions in embodied carbon relative to OPC have been reported; however, the magnitude of the benefit depends strongly on activator production, curing requirements, precursor processing, and system boundaries [4,5,9–12].

Despite the substantial number of publications in this field, most review articles are restricted either to individual categories of technogenic waste, such as mine tailings or metallurgical slags [13–17], or to specific aspects such as heavy-metal immobilization or the mechanical properties of the resulting materials. The decisive role of precursor mineralogy remains insufficiently resolved, particularly how phase composition governs the selection of an activation strategy and, consequently, the structure and service performance of the final product. The same bulk oxide composition can correspond to substantially different reactivity because Si, Al, Ca, Fe, Mg, and sulfate may occur in crystalline, amorphous, hydroxide, carbonate, or other mineral forms with different accessibility [18]. In some wastes, the intrinsic phase assemblage can be activated sufficiently to supply the species required for matrix or product formation [19–22]. In others, one or more required mineralogical functions remain deficient and must be supplied by a complementary solid precursor [23–26]. The central processing question is therefore not simply which oxide or gel family dominates, but whether the intrinsic mineral inventory is sufficient for the intended transformation and, if not, which mineralogical function must be compensated.

Current approaches to the classification of alkali-activated materials rely primarily on available Ca content and gel type, oxide-composition domains, or precursor origin [27–29]. More specialized studies have separately addressed mine tailings and Fe-rich precursors [30–32], whereas recent reviews of industrial wastes have largely retained a division into (Si + Al)- and (Si + Ca)-oriented compositions [9]. These approaches remain fragmented and do not provide a unified phase-oriented classification that simultaneously encompasses silicate phases; Fe-, Al-, Ca-, and Mg-bearing oxides and hydroxides; and sulfate phases, while linking their mineralogical functions to activation routes and reaction products.

The conventional low-Ca/high-Ca distinction remains useful because Ca availability strongly influences reaction kinetics and the tendency toward N-A-S-H-, C-(A)-S-H-, or hybrid gel formation, while gel-based classifications provide a convenient description of the reaction products ultimately formed [27–29,33–36]. However, these schemes are less informative when applied to heterogeneous mining and metallurgical wastes, because bulk Ca content does not indicate the mineral host, accessibility, or actual reactivity of Ca, Si, Al, Fe, or Mg, and several binding products may coexist within the same system. For example, the same copper-tailings matrix develops predominantly N-A-S-H-type products when combined with low-Ca fly ash, whereas Ca-rich blast-furnace slag shifts the reaction toward C-(A)-S-H/N-(C)-A-S-H products [25]. The mineralogy-guided framework proposed here therefore complements, rather than replaces, conventional Ca- and gel-based classifications by moving the analysis upstream from the final reaction product to the mineral inventory, phase accessibility, and mineralogical functions that control

processing and matrix development. Its main limitation is the need for sufficiently resolved mineralogical and reactivity data; where quantitative phase composition or phase-specific reactivity is unavailable, assignment remains necessarily less certain, particularly for highly heterogeneous and co-activated systems.

This review aims to systematize and synthesize current approaches for converting mining, metallurgical, and mixed industrial wastes into geopolymeric, alkali-activated, and related mineral matrices through a mineralogy-guided process-selection framework. Particular attention is paid to phase accessibility, the functional roles of individual mineral components, activation and pretreatment routes, reaction-product assemblages, final material form, durability, environmental stability, and application-specific performance. The analysis therefore links feedstock mineralogy with processing requirements and the minimum mineralogical functions needed to achieve the target product.

The primary organizing distinction used in this review is mineralogical sufficiency. Self-sufficient systems are those in which the waste itself provides the principal mineral inventory required for matrix or product formation, either directly or after activation of its intrinsic phases. When this inventory is insufficient or insufficiently accessible, mineralogical compensation is required through the addition of one or more functional mineral solids supplying deficient reactive Si, Al, Ca, sulfate, alkalinity, or other phase-forming contributions. Mineral phase families such as silicates, oxides, hydroxides, sulfates, and carbonates are treated as mechanistic descriptors rather than mutually exclusive precursor classes.

Accordingly, phase abundance alone is not used as an assignment criterion; where available, quantitative phase composition is interpreted together with evidence of phase dissolution, amorphization, reaction-product formation, and the functional role of the waste in the binder system.

2. Intrinsic Reactivity and Self-Sufficient Waste Systems

The conversion of mining, metallurgical, and other industrial wastes into solid mineral matrices is of particular interest because it can simultaneously reduce the volume of stored residues, replace a portion of primary mineral resources, and yield materials with specified structural, thermal-insulation, or functional properties. Such wastes can be used to manufacture binders, geopolymers, backfill materials, road-base materials, artificial aggregates, porous thermal-insulation products, and functional composites. Their ability to participate in the formation of a solid matrix, however, is governed less by the bulk contents of individual oxides than by phase state and the availability of reactive components [37,38].

Self-sufficient systems are defined as those in which the waste itself provides the principal mineral inventory required for matrix or product formation, either in its initial state or after activation that increases the accessibility of its own reactive phases. Their performance is therefore governed primarily by the mineralogical state, phase accessibility, and transformation of the waste itself. By contrast, when the intrinsic mineral inventory is insufficient or insufficiently accessible, additional solid precursors are introduced to compensate for deficient reactive Si, Al, Ca, sulfate, or other required components.

The principal self-sufficient transformation routes identified in the reviewed systems are summarized schematically in Figure 1, linking precursor mineralogy with activation strategy, structural evolution, and representative quantitative evidence.

For mineral tailings and slags, the mineralogical occurrence and accessibility of reactive phases are decisive. Silicon bound in quartz and resistant silicates participates only weakly in alkaline dissolution, whereas amorphous or glassy slag phases are generally more reactive. Their intrinsic reactivity can be enhanced through alkaline, thermal, mechanical, or other phase-transforming treatments.



Figure 1. Intrinsic activation and structural-evolution pathways in representative self-sufficient waste systems: (**a**) Cu-tailings reactivity and direct tile production [19,39], (**b**) thermally activated lithium slag [20], (**c**) thermally activated bauxite residue [21], and (**d**) pressurized carbonation of red mud [22]. Panel (**a**) integrates evidence from independent Cu-tailings studies and does not represent a single continuous experimental sequence. Created by the authors based on the cited studies.

Comparative dissolution studies of aluminosilicate minerals and industrial by-products demonstrate that similar bulk Si and Al contents do not imply similar alkaline reactivity: Crystallinity, bonding environment, and the fraction available for dissolution are decisive. Phase characterization should therefore precede activator selection and curing design. Accordingly, evidence was weighted according to the level of mineralogical resolution. Studies combining quantitative phase analysis, such as Rietveld-based XRD, with validated amorphous-phase quantification and dissolution or reaction-product data were considered the strongest basis for phase-specific interpretation [40–42]. Studies relying on qualitative XRD were interpreted more cautiously, whereas those reporting only bulk oxide chemistry were retained for compositional and performance comparisons but were not used alone to infer phase-specific reactivity or reaction mechanisms. This mineralogy-guided logic

has previously been identified as a key condition for applying geopolymerization in the mining and mineral-resources industries [43,44].

Table 1 compares representative self-sufficient waste systems in terms of their mineralogical roles, processing routes, product forms, quantitative performance, and potential applications.

The principal limitation of mineral tailings is the low availability of Si and Al. During alkaline-hydrothermal treatment of copper tailings, the activation energies for dissolution were 69.29 $kJ \cdot mol^{-1}$ for Si and 33.91 $kJ \cdot mol^{-1}$ for Al, indicating a stronger kinetic limitation on silicon release [19]. Alternatively, combining alkaline treatment with pressing produced a tile material whose dense structure was probably associated with the combined effects of chemical treatment and mechanical compaction [39]. Thus, the performance of sparingly soluble tailings can be controlled either by increasing phase accessibility or by physical forming; however, hydrothermal treatment should be justified by a commensurate improvement in reactivity.

A comparison of Cu-Ni, Cu-Zn, platinum-group-element, and iron-ore tailings confirmed the decisive role of mineralogy. Despite high SiO_2 contents in some samples, the tailings were predominantly crystalline and contained no XRD-detectable amorphous phase; after 24 h of alkaline leaching, less than 5% of the original components dissolved, compared with approximately 60% for ground-granulated blast-furnace slag (GGBFS) and 80% for metakaolin. Nevertheless, optimization of the activator and curing regime yielded up to 22 MPa for Cu-Ni tailings. Because geopolymer-gel formation was not demonstrated unambiguously, the strength may also have arisen from silicate binding, Ca-bearing hydrates, and particle densification [40]. For highly crystalline, low-reactivity tailings, compressive strength alone should not be considered evidence of geopolymerization. Chemical participation should be supported by converging evidence of precursor dissolution or phase consumption, formation of new binding products, and corresponding microstructural or spectroscopic changes. Where possible, comparison with unactivated or physically compacted controls should be used to separate chemical binding from particle-packing and filler/nucleation effects.

Recent work on high-volume iron-ore tailings (>80 wt%) showed that small additions of graphene oxide (GO) and MXenes can mitigate heterogeneous alkali activation by promoting glass-phase dissolution, strengthening particle–matrix interactions, filling microvoids, and reducing crack development. The proposed particle-chain structure illustrates how nanoscale additives can enhance the performance of a low-reactivity waste precursor, while their contribution should be distinguished from the intrinsic reactivity of the tailings themselves [45].

Early studies of copper tailings demonstrated the feasibility of producing shaped construction products through alkaline activation and mechanical compaction [46]. Subsequent investigations of durability and leaching showed that high initial strength alone cannot establish service or environmental acceptability [47]. These findings further support the separate evaluation of precursor reactivity, final product form, durability, and the immobilization of potentially hazardous components.

Compared with tailings, slags more often contain amorphous or metastable phases and may serve as independent precursors. Calcination of lithium slag at 700 °C increased the amorphous fraction from 15.9 to 48.1% and yielded a strength of 53.1 MPa. This case demonstrates that thermal amorphization can convert a low-reactivity residue into a viable sole precursor, although the gain in reactivity must be considered against the energy demand of calcination [20].

Table 1. Intrinsic mineralogical reactivity, direct activation routes, and performance of self-sufficient waste systems.

Waste-Derived System	Mineralogical Role	Key Processing Conditions	Product Form	Performance/Durability/ Leaching	Scale/Target Application	Ref.
Cu tailings	Quartz-dominated Si reservoir with limited bulk reactivity; Al is released more readily than Si.	Solid/liquid = 1:100; 1–6 M NaOH; 20–80 °C; 5–120 min; 1000 rpm.	Leaching slurry and alkali-treated residue; no hardened product.	Ea = 69.29 kJ·mol^{-1} (Si) and 33.91 kJ·mol^{-1} (Al); kinetics governed by product-layer diffusion/phase-boundary reactions.	Laboratory assessment of precursor reactivity for AAM design.	[19]
Cu tailings	Tailings serve as the sole solid precursor for directly shaped geopolymer tiles.	15 M NaOH; solution saturation 56.8%–57%; forming pressure 0.1–0.4 MPa; 105 °C for 48 h.	100 × 100 mm geopolymer tile prototype.	At 150 μm and 0.1 MPa: breaking load 986 ± 151 N; modulus of rupture 18.5 ± 0.7 MPa; water absorption 8.5 ± 1.5%.	Laboratory tile prototype. Embodied energy of 10.9 kWh·m^{-2}.	[39]
Cu/Ni-, Cu/Zn-, PGE-, and iron-ore tailings	Predominantly crystalline tailings with <5% dissolution; screening of activation and curing conditions.	Waterglass/NaOH activation; RT–60 °C; 7–28 d.	Hardened tailings-binder cylinders (Ø40 × 30 mm).	Cu/Ni tailings: 3.8–14.2 MPa at RT after 28 d; optimized formulations reached ~22 MPa.	Laboratory formulation screening. Proposed for on-site underground backfill; strength exceeds the cited 0.2–5 MPa range.	[40]
Li slag	Calcination increases the amorphous fraction, enabling sole-precursor geopolymerization.	Calcination at 700 °C; activator modulus = 1.2; alkali equivalent = 0.16; 28 d curing.	Sole-precursor geopolymer binder.	Amorphous fraction increased from 15.9% to 48.1%; 28 d compressive strength reached 53.1 MPa.	Laboratory-scale high-strength binder.	[20]
Bauxite residue (minimum-temperature activation)	Gibbsite dehydroxylation increases Al/Si accessibility and establishes the minimum calcination threshold.	BR dried at 110 °C for 24 h and calcined at 300–800 °C for 5 h; 8 M NaOH/Grade 52 sodium silicate; precursor:alkali = 70:30 or 65:35; moist-cured for 7–28 d.	BR geopolymer paste.	500 °C was the minimum solidification threshold and gave 23.15 MPa; calcined-BR pastes spanned 19.06–37.03 MPa, with the maximum at 800 °C.	Laboratory thermal-window screening. Identifies 500 °C as an energy-saving lower bound rather than defaulting to more energy-intensive activation.	[21]
RM (pressurized CO_2 mineralization)	RM alkalinity and Ca-bearing phases react with CO_2; hematite provides nucleation sites for carbonate precipitation and pore refinement.	Water/RM = 0.10; 30 × 10 mm pellets compacted at 6.25 N·mm^{-2}; 100% CO_2, 10 bar, 4 h; 25, 45 or 65 °C.	Carbonated RM pellets.	Strength +64%; CO_2 uptake 2.7 g/100 g RM; critical pore size 720→510 nm; shape retained after 56 d in water.	Laboratory CO_2-stabilized product. Mineralization reduced porosity (54.4% to 34.5%) and preserved pellet shape for 56 d in water.	[22]

Note: Values are not directly comparable because experimental conditions differ among studies. Durability and leaching outcomes are included where reported.

Silicomanganese slag illustrates the transition from structural to functional materials. Activation using a waste-glass-derived alkaline solution, together with the addition of 0.1%–1% carbon fibre, produced a composite with a temperature rise of 17–21.1 °C at 10 V [48]. In this case, the alkali-activated matrix provides mechanical integrity and the carbon fibres form a conductive network; practical applicability depends on resistance stability during cyclic heating and climatic exposure.

Self-sufficient conversion is not limited to silicate-rich tailings and slags. Thermal dehydroxylation of bauxite residue enabled direct alkali activation without a second mineral precursor; calcined-BR pastes developed compressive strengths of 19.06–37.03 MPa, while 500 °C represented the minimum reported solidification threshold [21]. A different direct route was demonstrated for red mud, where pressurized CO_2 mineralization utilized the intrinsic alkalinity and Ca-bearing phases of the residue. Carbonation increased strength by 64%, reduced porosity from 54.4% to 34.5%, and preserved pellet integrity after 56 d of water exposure [22]. These examples show that self-sufficiency is defined by utilization of the waste's own mineral inventory rather than by a specific oxide composition or gel family.

CO_2 mineralization should also be considered as an independent valorization route for Ca- and Mg-bearing residues. Carbonation capacity is controlled not by total CaO or MgO alone, but by mineral form, particle size, transport through the pore solution, product-layer passivation, pressure, temperature, and pretreatment [49,50]. Accordingly, reported uptake should be accompanied by reaction extent, energy demand, permanence of the carbonate products, and any changes in leaching or mechanical performance.

Carbonation is not universally beneficial. In Ca-rich alkali-activated matrices, prolonged or aggressive CO_2 exposure can decalcify C-(A)-S-H-type binding gels and reduce pore-solution alkalinity, potentially compromising the load-bearing matrix [36]. By contrast, controlled carbonation can be beneficial when carbonate precipitation predominantly fills pores and stabilizes reactive Ca/Mg-bearing phases, as observed for red mud [22]. The net effect therefore depends on whether carbonation primarily densifies the pore structure or consumes load-bearing binder phases; strength retention, phase evolution, porosity, and leaching should consequently be assessed before and after carbonation.

Taken together, these studies show that self-sufficient utilization is feasible when the waste contains sufficiently accessible reactive phases or when its intrinsic mineral inventory can be activated through thermal, alkaline, mechanical, or carbonation-based processing [19–22,39,40]. Where these approaches remain insufficient to provide the chemistry required for matrix formation or target performance, an additional mineral precursor becomes necessary.

3. Mineralogical Compensation in Binary and Multicomponent Systems

Mineralogical compensation is required in waste-derived systems whose intrinsic phase assemblage does not provide sufficient accessible species for matrix formation or target performance. Additional mineral solids are therefore introduced to supply deficient reactive Si, Al, Ca, sulfate, alkalinity, or other required components. Binary systems contain one additional matrix-forming or chemically functional mineral solid, whereas multicomponent systems combine two or more such components. Liquid activators, fibres, foaming agents, nano-additives, and inert aggregates are not counted as precursor components. A waste stream should not be treated merely as a source of one oxide; it has a resource–structure profile comprising mineral phases, the availability of Al, Fe, Ca, Mg, and sulfate, particle-size distribution, and the presence of potentially hazardous components. Phase-specific characterization is equally important for sulfur-bearing industrial residues. For example, sulfur cake from sulfuric-acid production contains a high total sulfur content, while gypsum, calcium sulfate, and silicate phases occur only in minor quantities, illus-

trating why bulk elemental composition alone cannot be used to infer the availability of a functional sulfate source [51]. In another example, red mud may simultaneously provide alkali, Fe/Al-bearing phases, and nucleation sites, whereas slag may supply reactive Ca and amorphous silicate. These roles explain why chemically complementary blends often outperform single-waste formulations [52–54].

Figure 2 summarizes three representative compensation strategies, showing how targeted functional addition, compositional synergy, and integrated precursor processing modify reaction pathways and material performance.

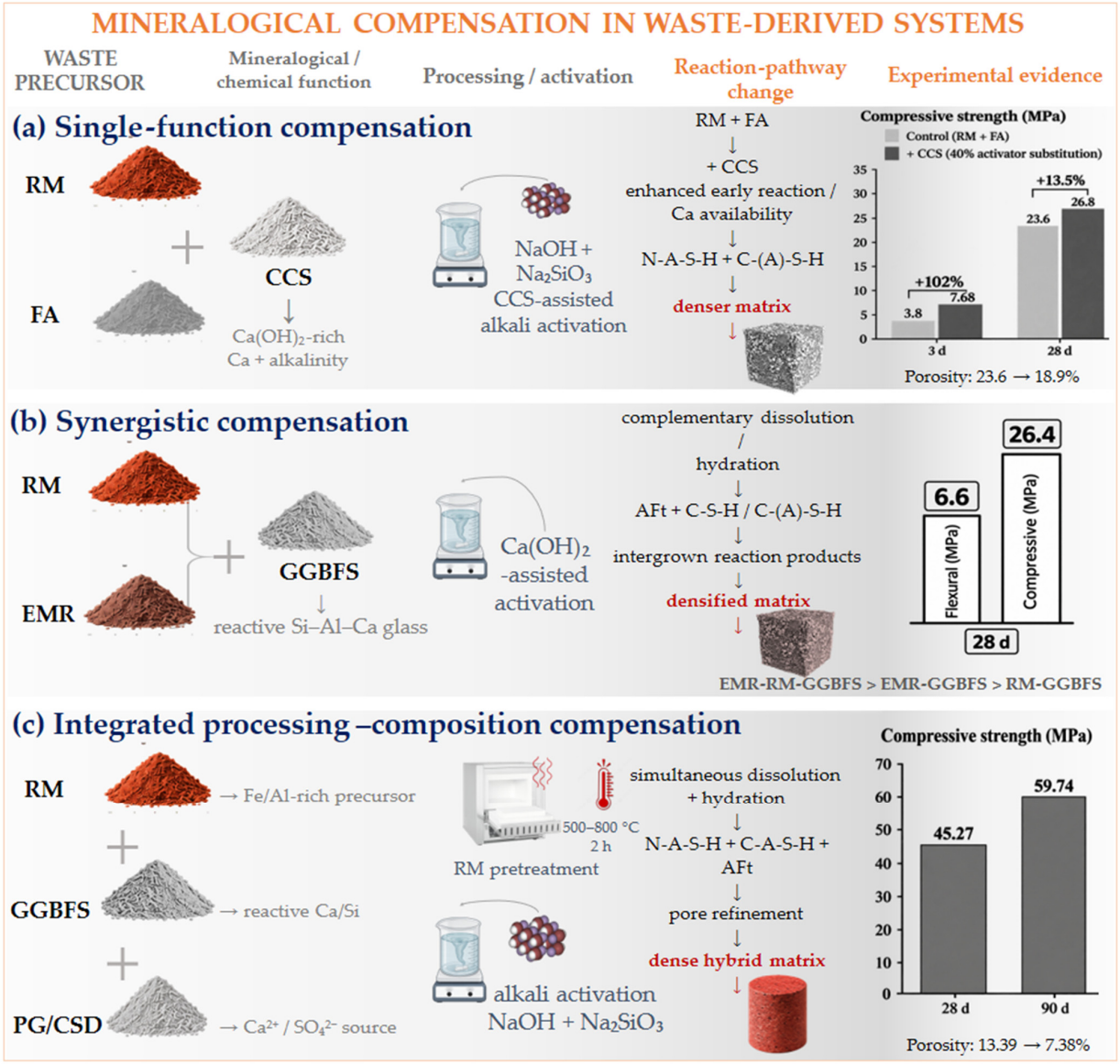


Figure 2. Representative mineralogical-compensation strategies in waste-derived systems: (**a**) targeted single-function compensation using calcium-carbide slag in a red-mud/fly-ash system [26]; (**b**) synergistic compositional compensation in an EMR/red-mud/GGBFS system [55]; and (**c**) integrated processing–composition compensation through red-mud pretreatment followed by GGBFS/CSD addition [56]. The scheme links precursor functions, processing, reaction-pathway changes, and quantitative experimental evidence. Created by the authors based on the cited studies.

Table 2 summarizes representative binary systems in which a second mineral component compensates for limited phase accessibility, deficient matrix-forming species, or insufficient durability of the original waste-derived precursor.

Table 2. Mineralogical compensation, processing routes, and performance of binary waste-derived systems.

Waste-Derived System	Mineralogical Role	Key Processing Conditions	Product Form	Performance/Durability/Leaching	Scale/Target Application	Ref.
Mo tailings + slag	Hydrothermal treatment activates quartz-rich tailings, producing a reactive sodium aluminosilicate precursor.	5 M NaOH, 200 °C, 4 h; 80 wt% activated tailings + 20 wt% slag; w/s = 0.40.	Dry one-part precursor blend and hardened 30 mm cubes.	Si leaching increased from 35.4 to 1046.8 mg·L^{-1} (29.6×); an amorphous C-(N)-A-S-H/N-(C)-A-S-H-containing matrix developed.	Laboratory-scale one-part binder. 80 wt% activated tailings.	[57]
Cu mine tailings + PC	Cement stabilization improves resistance of tailings to seasonal freeze–thaw and wet–dry degradation.	4–12 wt% Type III Portland cement; up to 12 freeze–thaw and 12 wet–dry cycles.	Compacted stabilized tailings specimens.	After 12 freeze–thaw cycles, stabilized tailings retained 39%–55% of initial strength; after wet–dry cycling, 16%–34% was retained.	Laboratory durability validation under simulated seasonal exposure.	[58]
Li slag + $Ca(OH)_2$	Reactive Si/Al from lithium slag participates in matrix formation, while $Ca(OH)_2$ supplies alkalinity and Ca, shifting the reaction pathway toward C-(A)-S-H and ettringite formation.	20 wt% $Ca(OH)_2$; L/S = 0.40; binder:sand = 1:3; ambient curing (>95% RH) or 60 °C for 24 h.	Zero-cement, dry-activated mortar/binder.	Optimum 20 wt% $Ca(OH)_2$ system achieved 38.22 MPa at 28 d under ambient curing.	Laboratory-scale zero-cement mortar with ambient hardening.	[59]
Li slag + PC	Low-alkali polymetallic salts complement deficient Ca/Al/Si supply and promote C-(A)-S-H/N-A-S-H co-gels and AFt.	50 wt% lithium slag + 50 wt% Portland cement; water/solid = 0.60; 6 wt% composite activator; 20–25 °C; 7–21 d.	Low-alkali, high-volume lithium-slag cement paste.	Compressive strength increased by 306%, 123%, and 108% at 7, 14, and 21 d, respectively, while CO_2 emissions per unit strength decreased by 52.2%.	Laboratory-scale low-carbon cementitious binder. Multi-element activation restores strength at 50 wt% slag while avoiding highly caustic activator solutions.	[60]
Fe tailings + MK	Metakaolin (MK) provides the principal reactive Si–Al source, while iron tailings partially replace MK and act mainly as supplementary mineral/filler components in the foamed geopolymer matrix.	10–20 wt% iron tailings replacing MK; foamed with Al powder, H_2O_2 or sodium perborate; properties evaluated to 90 d.	Lightweight foamed geopolymer block/panel.	Sodium perborate: k = 0.110–0.211 W·m^{-1}·K^{-1} and 1.5–5 MPa; Al powder: strength up to 13 MPa.	Laboratory-scale insulation material. Foaming chemistry permits strength–thermal-conductivity tuning; 20 wt% tailings can improve mechanical response.	[61]

Table 2. *Cont.*

Waste-Derived System	Mineralogical Role	Key Processing Conditions	Product Form	Performance/Durability/ Leaching	Scale/Target Application	Ref.
Ilmenite tailings + MK	Tailings supply Fe/Ca-bearing phases while metakaolin supplies reactive Si/Al; H_2O_2 generates a hierarchical pore network.	0–20 wt% tailings; 2–4 wt% H_2O_2; activator modulus = 1.2; alkali equivalent = 11%; L/S = 0.35–0.39.	Alkali-activated foam/thermal-insulation panel material.	Across optimized formulations, porosity reached 73.32%, pore connectivity 99.98%, compressive strength 1.20 MPa, and the minimum measured thermal conductivity was 0.0602 $W \cdot m^{-1} \cdot K^{-1}$.	Laboratory-scale insulation foam. Highly connected multiscale porosity yields very low thermal conductivity at usable lightweight strength.	[62]
Mo + FA	Ultrafine tailings contribute Si-bearing fines, while fly ash supplies reactive aluminosilicate for N-A-S-H formation.	Molybdenum tailings (MoT):FA = 300:0–0:300; 200 min grinding; 3–12 M NaOH; w/s = 0.36–0.42; 85 °C for 6–48 h; tested at 3–28 d.	Hardened geopolymer paste/cubes.	Optimum (MoT:FA = 1:4; 9 M; w/s = 0.40; 48 h) reached 31.26 MPa at 28 d; 501.67–765.74 kg CO_2e m^{-3} versus 1403.81 for OPC.	Laboratory-scale low-carbon binder. Couples N-A-S-H strength development with a substantially lower cradle-to-gate carbon indicator than OPC.	[63]
Phosphate mine tailings/sludge + FA	$CaCO_3$-/phosphate-bearing tailings partially replace fly ash and become immobilized within the geopolymer matrix.	10–30 wt% tailings replacing FA; 225 g sodium silicate per 450 g precursor; w/b = 0.45; 40 mm mortar cubes; 60 °C; 1–28 d.	Geopolymer construction mortar.	At 30 wt% tailings: 59 MPa at 28 d and indentation hardness 1.05 GPa; reported immobilization efficiencies were generally >98%.	Laboratory-scale construction mortar. Combines high strength with stabilization of potentially hazardous constituents.	[64]
Cu + FA or BFS	Low-Ca FA favours N-A-S-H, whereas Ca-rich BFS promotes faster C-(A)-S-H/N-(C)-A-S-H formation in sulfate-bearing tailings.	precursor/(tailings + precursor) = 0.30–0.50; NaOH ~10 M (FA) or ~6 M (BFS); 85 °C (FA) or 40 °C (BFS); accelerated curing.	Compacted, stabilized tailings-binder cylinders.	Top BFS formulation reached ~15 MPa at 28 d; top FA formulation reached ~11 MPa; shortlisted mixes emitted 0.21–0.52 kg CO_2e kg^{-1} paste.	Laboratory screening; proposed end use. Supports mix optimization for underground backfill/building materials, with BFS providing higher early UCS (unconfined compressive strength).	[25]

Table 2. *Cont.*

Waste-Derived System	Mineralogical Role	Key Processing Conditions	Product Form	Performance/Durability/ Leaching	Scale/Target Application	Ref.
Bioleached sulfidic mine tailings + BFS	Bioleached tailings act mainly as a filler in a reactive slag matrix while the binder encapsulates residual sulfides/metalloids.	20–50 wt% tailings replacing BFS; precursor:solid sodium metasilicate = 9:1; w/b = 0.35; sand/binder = 2; 23 °C, RH 90%; 28–90 d.	One-part alkali-activated slag mortar.	At 50 wt% tailings, compressive strength reached 51.8 MPa at 28 d and 52.6 MPa at 90 d.	Laboratory-scale high-strength mortar. One-part processing combines high tailings loading, strong mechanical performance and contaminant retention.	[65]
RM + FA	Fe/Al-rich red mud supplies alkali and Al but limited reactive Si; fly ash balances Si. Calcination increases reactivity in a source-dependent manner.	Five RM sources; 800 °C/2 h; RM:FA = 25:75–75:25; 4–12 M NaOH; sodium silicate/precursor = 0.37; water/precursor = 0.12; 60 °C/24 h then ambient curing.	Hardened geopolymer paste cubes and companion alkali-leached precursor.	At 50 wt% RM and 8 M NaOH, 28 d UCS exceeded 40 MPa; thermal-treatment gain ranged from <1 to ~21 MPa across RM sources.	Laboratory source/activation screening. Defines source-specific quality-control and alkali windows; thermal pretreatment is beneficial but not universally transferable among red muds.	[52]
RM + FA	Red mud contributes Fe/Al/Ca and intrinsic alkali, while fly ash supplies the reactive Si/Al required for the geopolymer network.	FFA:RM = 4:1; Si/Al = 2.0; Na/Al = 0.6; 50 wt% NaOH:2 M sodium trisilicate:water = 3:7:3; 23 °C/28 d; pH 3 or 7 exposure for 1–120 d.	Geopolymer cylinders and prisms for durability and leaching tests.	UCS: 10 ± 1.6→6.7 ± 1.9 MPa after 7 d acid exposure; ~6–7 MPa at 28–120 d; heavy-metal leaching below cited limits.	Laboratory durability benchmark. Showed low-pH resistance comparable to the OPC control; reported heavy-metal leaching remained below the cited US EPA soil limits.	[53]
Alkali-thermally activated bauxite residue + silica fume	Bauxite residue provides Al and retained alkali; silica fume corrects its Si deficiency for water-activated one-part geopolymerization.	BR ground <90 μm and fused with 10%–20% Na_2O at 800 °C/1 h; 10%–40% silica fume; L/B = 0.45; 0.5% superplasticizer; ambient preparation/curing.	Water-added one-part geopolymer paste and 50 mm cubes.	Optimum BR22 (15% Na_2O, 20% silica fume) reached 19 MPa at 28 d; higher silica-fume contents caused microcracking and strength loss.	Laboratory-scale one-part binder. Enables water-only final mixing and identifies a practical Si/alkali balance for BR solidification.	[54]

Table 2. *Cont.*

Waste-Derived System	Mineralogical Role	Key Processing Conditions	Product Form	Performance/Durability/ Leaching	Scale/Target Application	Ref.
RM + slag artificial aggregate	Alkali-activated RM/slag forms a cold-bonded core; a cement shell provides secondary curing and enables aggregate use in concrete.	Optimum core: 70% RM + 30% slag; waterglass modulus = 1.8; alkali equivalent = 7%; cement shell; RMAC at w/c = 0.28 and 50% RMA replacement.	Non-sintered core–shell artificial aggregate and aggregate concrete.	Optimized activated matrix reached 39.1 MPa compressive and 7.4 MPa flexural strength at 28 d; optimum RMAC reached 19.1 MPa.	Laboratory aggregate/concrete prototype. Converts RM into a directly usable aggregate without high-temperature sintering; 50% replacement gave the best concrete response.	[66]
Modified magnesium slag + FA	Mechanical grinding increases lattice defects and amorphization in modified Mg slag, activating a clinker-free backfill binder.	80% solids; 20% MMS binder + 30% high-Ca FA + 50% aeolian sand; 20 °C and ≥95% RH; 3–28 d.	Cement-free paste-backfill slurry and 70.7 mm mortar cubes.	A 60 min optimum gave 503 $m^2 \cdot kg^{-1}$ specific surface and 3.83% residue on 45 μm; most UCS gain occurred by 60 min, with little benefit up to 120 min.	Laboratory process optimization; field-use context reported. Balances grinding energy, fluidity and reactivity for a Portland-cement-free coal-mine backfill route.	[67]
Fe-rich fayalite slag + ladle slag or BFS	Fayalite slag is the main Fe-rich precursor and aggregate; 20 wt% Ca/Al-rich co-binder modifies gels and limits frost/chemical degradation.	100% FS or 20% binder replacement by LS/BFS; granular FS aggregate:binder = 2; 10 M NaOH + sodium silicate; 23 °C; 180 freeze–thaw cycles in water, pH 1 acid or sulfate–chloride solution.	Alkali-activated Fe-rich mortar cubes and prisms.	After 180 cycles, sole-FS mortar disintegrated; 20% LS/BFS blends retained their form with partial damage.	Laboratory durability screening. Shows that co-binder addition is essential for aggressive/cold service; the durability gain must be balanced against higher drying shrinkage.	[68]

Note: Values are not directly comparable because experimental conditions differ among studies. Durability and leaching outcomes are included where reported.

The role of tailings in the matrix depends on processing intensity and overall formulation. Molybdenum tailings treated with 5 M NaOH at 200 °C for 4 h were combined with slag; the supply of reactive Ca and amorphous Si promoted the formation of a C-(N)-A-S-H-containing matrix, showing that the outcome was controlled by chemical complementarity rather than the independent reactivity of the tailings [57]. By contrast, at low gold-tailings contents in cementitious composites, their contribution was probably limited to pore filling, nucleation, and partial pozzolanic reaction; in this case, the resource benefit depends on the actual displacement of clinker [69].

With additions of 4, 8, and 12 wt% Type III Portland cement, 39, 50, and 55% of the initial strength, respectively, were retained after 12 freeze–thaw cycles [58]. Increasing the cement dosage improved resistance but did not prevent substantial degradation, thereby limiting the use of such formulations without further optimization of pore structure and water resistance.

Lithium slag further illustrates how a second mineral component can redirect reaction chemistry. Addition of 20 wt% $Ca(OH)_2$ supplied both alkalinity and reactive Ca, producing 38.22 MPa at 28 d without Portland cement [59]. In a separate formulation containing 50 wt% Portland cement, low-alkali silicate–sulfate activation promoted C-(A)-S-H/N-A-S-H co-gels and AFt while reducing the reported CO_2 indicator per unit strength by 52.2% [60].

In porous materials, the chemical complementarity of precursors is coupled with gas-evolution control and cell stability. For iron tailings combined with metakaolin, sodium perborate produced a thermal conductivity of approximately 0.110 $W \cdot m^{-1} \cdot K^{-1}$ at strengths of 1.5–5 MPa, whereas Al powder increased the strength to 13 MPa [61]. For ilmenite tailings foamed with H_2O_2, a porosity of 73.3% and pore connectivity of 99% reduced thermal conductivity to approximately 0.060 $W \cdot m^{-1} \cdot K^{-1}$, but the strength was only 1.20 MPa [62]. The performance of geopolymer foams is therefore governed not by maximum porosity, but by the balance among thermal conductivity, strength, and moisture resistance [70].

Nanoscale modification provides an additional means of controlling the strength–porosity–durability balance in porous geopolymers. In graphene-oxide-reinforced geopolymer foam concrete, the maximum compressive strength reached 2.958 MPa, representing a 58.37% increase, while 0.06 wt% GO reduced freeze–thaw mass loss and compressive-strength loss by 51.2% and 41.1%, respectively; these improvements were associated with nucleation, matrix connectivity, and pore refinement [71].

Mechanochemical treatment of mica- and carbonate-bearing phosphate tailings enabled waste contents of up to 70 wt% and strengths above 20 MPa. Natrolite and cancrinite formed alongside N-A-S-H and C-(N)-A-S-H gels, indicating a more complex structural evolution than the formation of an amorphous matrix alone [72]. In a molybdenum-tailings/fly-ash system, optimization of alkalinity, water-to-solid ratio, and thermal curing yielded 31.26 MPa and N-A-S-H formation [63]. Both examples show that high tailings contents are achieved either by increasing structural disorder or by combining the tailings with a more accessible aluminosilicate source. Phosphate tailings or sludge combined with fly ash yielded a strength of 59 MPa and a hardness of 1.05 GPa, although the contribution of the tailings must be distinguished from that of the more reactive fly ash [64].

The role of a Ca-bearing co-precursor is particularly evident in BFS-containing systems. Slag-based copper-tailings formulations reached approximately 15 MPa, compared with 11–12 MPa for fly-ash-based formulations [25]. In bioleached sulfidic tailings combined with BFS, the 20 wt% tailings formulation reached 91.1 MPa at 90 d, whereas the 50 wt% formulation reached 51.8 MPa at 28 d and 52.6 MPa at 90 d [65]. The strength gain provided by BFS does not, however, eliminate the need to control residual sulfides, acid-generation potential, and metal leaching.

Binary compensation in red-mud- and bauxite-residue-based systems is strongly dependent on the mineralogical state of the primary waste. Thermal pretreatment of five red-mud sources followed by blending with fly ash produced markedly source-dependent gains in reactivity and strength, with the effect of calcination ranging from less than 1 to approximately 21 MPa [52]. In a red-mud/Class F fly-ash system, fly ash supplied the reactive Si/Al required for matrix development, while long-term acid exposure revealed substantial losses in mechanical properties despite acceptable heavy-metal retention [53]. Alkali-thermally activated bauxite residue combined with silica fume provides another form of binary compensation, in which the Si-rich addition corrects the limited silicate availability of the residue; the optimum formulation reached approximately 19 MPa [54].

Low-Ca ferronickel slag can participate in geopolymerization when combined with an alkali-soluble silicate source [73], while the conversion of heterogeneous wastes more generally proceeds through coupled dissolution, transport, and precipitation reactions [74].

Binary compensation can also support product forms beyond conventional binder pastes. Red mud combined with slag was converted into cold-bonded artificial aggregate, with the resulting concrete reaching 19.1 MPa [66]. In a modified-magnesium-slag/fly-ash backfill system, mechanical activation increased the specific surface area to 503 $m^2 \cdot kg^{-1}$, although most of the reactivity gain was achieved within the first 60 min of grinding [67]. These cases show that the benefit of a second mineral component depends not only on reaction chemistry but also on the intended forming and application route.

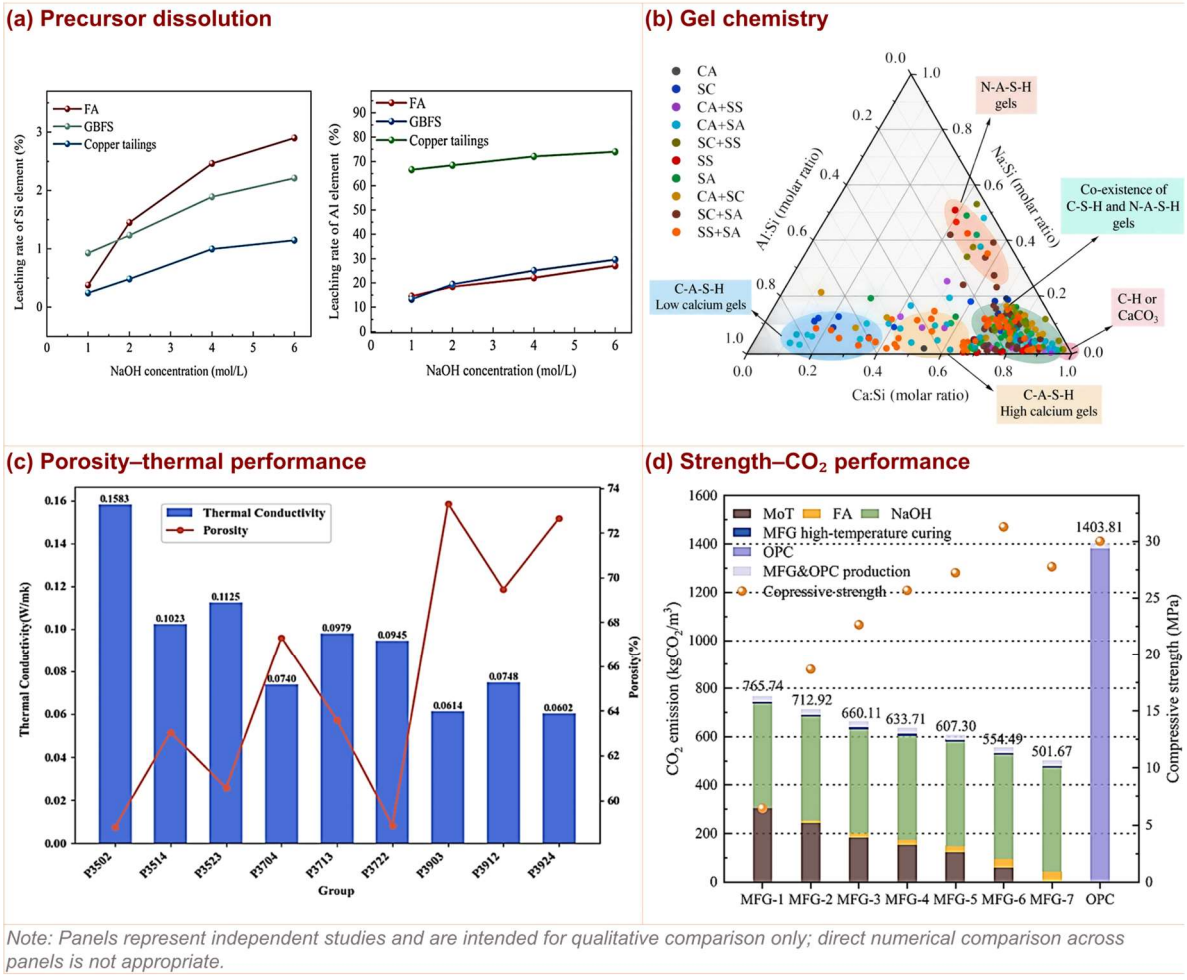
Durability data reveal limitations that are not evident from initial strength. After 180 freeze–thaw cycles in water, alkali-activated fayalite-slag mortar without a co-precursor failed completely, whereas BFS- and ladle-slag-modified variants retained approximately 20 and 30 MPa, respectively [68]. Under 120 d of exposure to H_2SO_4 at pH 3, a red-mud/fly-ash material lost approximately 30% of its compressive strength, 45% of its flexural strength, and 70% of its Young's modulus [53]. These results confirm that co-precursor selection must be assessed through long-term transport and degradation mechanisms, not only early-age strength.

Representative experimental evidence linking precursor dissolution, gel chemistry, functional performance, and environmental trade-offs is summarized in Figure 3.

Figure 3 illustrates how mineralogical reactivity and binary compensation are reflected in precursor dissolution, reaction-product chemistry, pore structure, and environmental performance. In Figure 3a, increasing NaOH concentration enhances Si and Al release, although the increase gradually levels off at high alkalinity. Copper tailings exhibit comparatively high Al leaching but much lower release of Si, which is bound predominantly in resistant quartz. A high Al concentration in solution is therefore not an independent measure of geopolymer reactivity, because formation of a binding matrix requires a balanced supply of soluble Si and Al [19]. Figure 3b further demonstrates that structure development is not limited to a single gel type. After 21 d, C-S-H-, C-A-S-H-, and N-A-S-H-like products may coexist depending on the Ca/Si, Al/Si, and Na/Si ratios. A Ca-bearing environment favours C-(A)-S-H formation, whereas Na-bearing activators enhance N-A-S-H formation. Activator chemistry and the ratios of available Ca, Na, Si, and Al are therefore more informative than the formal classification of the initial waste [60]. The transition to porous materials changes the optimization criterion: As shown in Figure 3c, increasing porosity reduces measured thermal conductivity to approximately 0.060 $W \cdot m^{-1} \cdot K^{-1}$ but simultaneously limits strength, which was approximately 1.20 MPa for the highly porous formulation. For thermal-insulation materials, the optimum is therefore not maximum gas generation, but a controlled, uniform pore structure that provides an acceptable balance between thermal conductivity and mechanical stability [62].

Finally, Figure 3d shows that a high waste fraction does not automatically guarantee a low carbon footprint. For geopolymers prepared from molybdenum tailings and fly

ash, calculated emissions ranged from 501.67 to 765.74 kg CO_2-eq m^{-3}, compared with 1403.81 kg CO_2-eq m^{-3} for OPC; however, a substantial fraction of the impact arose from NaOH production, mechanical grinding, and high-temperature curing. Environmental benefit must therefore be evaluated together with strength and processing intensity using consistent life-cycle boundaries [63]. Collectively, these cases show that mineralogical compensation cannot be evaluated from a single performance metric: Improved phase accessibility must translate into appropriate reaction products, product architecture, and environmental performance.



Note: Panels represent independent studies and are intended for qualitative comparison only; direct numerical comparison across panels is not appropriate.

Figure 3. Representative process–structure–performance relationships illustrating mineralogical reactivity and binary compensation: (**a**) precursor dissolution [19], (**b**) reaction-product chemistry [60], (**c**) porosity–thermal performance [62] and (**d**) strength–CO_2 performance [63]. The panels represent independent case studies and are not intended for direct quantitative comparison. Adapted from Refs. [19,60,62,63] with permission.

Binary compensation is effective when one additional mineral component can correct the dominant limitation of the original waste, for example, by supplying reactive Si/Al, Ca, alkalinity, or a more reactive binding phase. More heterogeneous systems, however, may require several complementary solids to provide different phase-forming species simultaneously. In such multicomponent formulations, performance depends on engineered mineralogical complementarity rather than on the contribution of a single additional precursor. Table 3 summarizes representative multicomponent systems in which several mineral solids perform complementary chemical or structural functions.

Table 3. Engineered mineralogical complementarity, processing routes, and performance of multicomponent waste-derived systems.

Waste-Derived System	Mineralogical Role	Key Processing Conditions	Product Form	Performance/Durability/ Leaching	Scale/Target Application	Ref.
RM + FA + CCS	$Ca(OH)_2$-rich carbide slag partially replaces the conventional alkali activator and promotes coexisting C-(A)-S-H and N-A-S-H gels.	FA:RM = 6:4; effective activator = 25% of precursor; CCS replaces 0%–100% of NaOH-based activator; L/S = 0.52; 20 °C and 98% RH; optimum CCS substitution = 40%.	Red mud–fly ash geopolymer paste cubes.	At 40% CCS substitution: 7.68 MPa at 3 d and 26.8 MPa at 28 d, increases of 102% and 13.5% over the control, respectively.	Laboratory-scale waste-activated binder. Partly replaces commercial alkali, increases early strength and suppresses efflorescence through early Ca-bearing gel formation.	[26]
Ferronickel slag + BFS + FA	Fe/Mg-bearing FNS is the slower-reacting waste fraction; Ca-rich BFS accelerates C-A-S-H formation and FA improves particle packing and flow.	FNS:BFS:FA = 20:50:30; W/B = 0.40; NaOH + sodium silicate (SiO_2/Na_2O = 1.2); 1% water reducer; 20 °C, >95% RH; 1–28 d.	Cement-free geopolymer grout and injected medium-sand body.	Binder reached 69.6 MPa at 28 d with 317 mm flow; grouted sand reached 5.7 MPa at 1 d and 9.36 MPa at 14 d.	Laboratory grouting simulation. Demonstrated injectability and consolidation of medium sand while using an all-solid-waste ternary precursor.	[75]
Calcined red mud + GGBFS + PG	Calcined RM supplies Fe/Al-rich precursor, GGBFS supplies reactive Ca/Si, and phosphogypsum supports sulfate-bearing reaction products and pore refinement.	RM calcined at 500–800 °C (2 h hold); 12 M NaOH; $Na_2SiO_3/NaOH$ = 1.5; activator/binder = 0.47; 80 °C/24 h then 25 °C.	Geopolymer concrete cylinders and prisms.	45.27 MPa at 28 d and 59.74 MPa at 90 d; water absorption 3.11%, porosity 7.38%; improved chloride/freeze–thaw resistance.	Laboratory-scale durable concrete. The hybrid N-A-S-H/C-A-S-H matrix improved strength, chloride resistance and freeze–thaw performance at 40 wt% RM.	[56]
EMR + RM + GGBFS	EMR-derived sulfate promotes AFt, RM supplies intrinsic alkali, and GGBFS supplies reactive Ca/Si for C-(A)-S-H formation.	E-R-G = 20% EMR + 15% RM + 55% GGBFS + 10% $Ca(OH)_2$; water/binder = 0.50; paste cubes and 40 × 40 × 160 mm mortar prisms; 3–28 d.	Multi-waste cementitious paste and mortar.	Ternary E-R-G reached 26.4 MPa compressive and 6.6 MPa flexural strength at 28 d, outperforming the corresponding binary systems.	Laboratory-scale synergistic binder. Pairs the acidity/sulfate of EMR with RM alkalinity, increasing AFt and C-S-H while reducing the need for a single high-dose activator.	[55]
EMR + coal slag + GGBFS	EMR supplies sulfate, coal slag supplies Si/Al, and GGBFS supplies reactive Ca; NaOH drives C-(A)-S-H/N-A-S-H co-gel formation.	20% GGBFS; EMR = 10%–55%; coal slag = 25%–70%; 14 wt% NaOH solution; W/C = 0.55; 20 °C and ≥95% RH; 28 d then groundwater/ 5% $NaCl/Na_2SO_4$ exposure.	Alkali-activated grouting slurry and hardened prisms/cubes.	28 d compressive/flexural strength 16.2–19.3/ 5.9–7.0 MPa; residual-strength factors >0.97/>0.93; leaching met cited limits.	Laboratory durability assessment for grout. Reported leaching met the cited national limits; estimated cost was 1250 RMB t^{-1} and carbon emissions 84.86 $kg{\cdot}t^{-1}$.	[76]

Table 3. *Cont.*

Waste-Derived System	Mineralogical Role	Key Processing Conditions	Product Form	Performance/Durability/ Leaching	Scale/Target Application	Ref.
RM–FA-based binder for aeolian-sand backfill	Aeolian sand forms the aggregate skeleton; RM supplies fine Al/alkali-bearing particles and FA supplies reactive spherical aluminosilicate for flow and strength.	50% aeolian sand; 3% OPC; Na_2O = 3%; activator modulus = 1.6; FA:RM = 1–5; solids = 78% or 80%; 20 °C and 95% RH.	Aeolian-sand/RM/FA cemented paste-backfill slurry and specimens.	28 d UCS 5.6–6.4 MPa; B4 leachate met cited Class III groundwater limits.	Laboratory-scale mine backfill. Combines pumpable rheology with strength above the study's backfill requirement while co-utilizing RM, FA and local sand.	[77]
GGBFS–EMR–OPC binder for engineering-sediment stabilization	The GGBFS–EMR–OPC binder couples latent slag reactivity, EMR sulfate and limited clinker hydration to stabilize urban sediment.	Optimum GGBFS:EMR:OPC = 5:3:2; 5%–10% binder; water content = 17.5%; compacted 50 × 50 mm cylinders; 23 °C and 95% RH.	Compacted stabilized sediment for road subgrade.	28 d UCS >8 MPa; CO_2 and cost reduced by 84.5% and 67%; acceptable leaching after water/ sulfate exposure.	Laboratory-scale subgrade material. Meets the cited road-solidified-soil strength criteria with lower binder/OPC demand and acceptable leaching after water/sulfate exposure.	[78]
Oil-shale residue + steel slag + soda residue	Soda residue supplies Ca^{2+}/OH^{-}, while oil-shale residue and steel slag provide complementary silicate/aluminate phases for cement-free hydration.	No cement or chemical additives; optimum soda residue = 12%; solids = 70.32%; steel slag:oil-shale residue = 1.17; water-only mixing; 20 °C and 96% RH.	All-solid-waste low-carbon cemented backfill slurry/body.	28 d UCS 5.97 MPa; slump 205 mm; CO_2 86.9% lower; Class III-compliant heavy-metal leachate.	Laboratory-optimized mine backfill. Uses 100% solid-waste binder, meets the study's filling-performance criteria, and produced Class III-compliant heavy-metal leachate.	[79]
Thermally modified EMR + GG-BFS/CCS/clinker	Low-temperature treatment converts EMR gypsum to a more reactive sulfate activator; CCS and clinker support GGBFS hydration and sealing.	EMR at 300 °C/2 h; composite activator = modified EMR:CCS:clinker = 25:3:4; optimum activator content = 25%; W/B = 0.80; 28 d then 21 wet–dry cycles.	EMR–GGBFS cement grout/karst sealing body.	Permeability 9.3×10^{-8} cm·s^{-1}; minimum UCS loss 3.69% after 21 leachate wet–dry cycles.	Laboratory karst-environment simulation. Meets the cited $<10^{-7}$ cm s^{-1} landfill anti-seepage threshold and showed the best resistance to EMR leachate at the 25% optimum.	[80]

Table 3. *Cont.*

Waste-Derived System	Mineralogical Role	Key Processing Conditions	Product Form	Performance/Durability/ Leaching	Scale/Target Application	Ref.
Full-solid-waste binder for aeolian-sand subgrade	Carbide slag supplies Ca/OH^{-}, while GGBFS, fly ash, silica fume and desulfurization gypsum provide complementary Ca–Si–Al–sulfate modules.	Binder mass ratio = 4:3:2:3:2; 0–40 wt% binder; no external alkali; compaction = 94%–100%; UCS, CBR, water stability, freeze–thaw and leaching tests.	Compacted, stabilized aeolian-sand road-subgrade material.	28 d UCS 6.88 MPa; resilient modulus 1.98× and CBR 1.53× higher; no reported heavy-metal hazard in leaching tests.	Laboratory-scale road-subgrade material. Uses a 100% industrial-solid-waste binder without external strong alkali and showed no reported heavy-metal hazard in the leaching assessment.	[81]
EMR + vanadium-bearing shale leaching residue + BFS	Alkali-thermo-mechanically activated EMR supplies sulfate/alkali, while the leaching residue and BFS provide complementary oxide modules for hybrid gel formation.	Alkali–thermal–mechanical pretreatment; water-added one-part formulation; 14 d and autoclave-dry curing.	Water-added one-part geopolymer binder/hardened composite.	Compressive strength reached 23.8 MPa at 14 d and a maximum of 35.1 MPa after autoclave-dry curing; C-S-H and N-(C)-A-S-H formed synergistically.	Laboratory-scale one-part hybrid binder. Avoids handling a separate corrosive liquid activator at final use and co-utilizes two metal-processing residues.	[82]
Wet bauxite residue + FA + waste glass	Wet BR provides Al and intrinsic alkalinity; waste glass supplies amorphous Si and replaces fly ash to tune gel cross-linking and salt-scaling resistance.	Filter-pressed BR (36% water), used without drying/grinding; glass replaces 0%–100% FA; activator/binder = 0.40; 50 cycles at −18 °C/16 h and 4 °C/8 h in 4% $CaCl_2$.	Hardened BR-based geopolymer specimens for cold-region scaling.	Strength +17%; scaling mass loss −48%; cumulative scaled mass 0.32 $kg \cdot m^{-2}$ after 50 cycles.	Laboratory cold-region durability material. RF75 balances strength and deicer-salt scaling resistance; RF100 maximizes glass use for lower-load/nonstructural applications.	[83]
RM + waste glass + PC	Red mud supplies Al and intrinsic alkali, glass powder supplies Si, and a small cement fraction adds Ca-bearing hydration products.	RM:glass = 1.5; 0, 2.5 or 5 wt% cement; water, 4 M or 8 M NaOH; L/S = 0.45–0.50; 24 °C/28 d.	One-part or alkali-activated ternary geopolymer cylinders.	Water-only GP7 (57% RM, 38% glass, 5% cement) reached 11.35 ± 1.23 MPa at 28 d; increasing added NaOH reduced strength.	Laboratory-scale low-alkali binder. Uses the intrinsic alkalinity of RM; the best mix required only water at final mixing, whereas excess alkali promoted efflorescence.	[84]

Note: Values are not directly comparable because experimental conditions differ among studies. Durability and leaching outcomes are included where reported.

Multicomponent compensation can extend beyond the addition of conventional co-precursors by incorporating waste-derived activating solids. In the red-mud/fly-ash system, $Ca(OH)_2$-rich carbide slag partially replaced NaOH while promoting coexisting Ca- and Na-aluminosilicate products; 40% replacement yielded 26.8 MPa at 28 d [26]. This illustrates how a third functional solid can simultaneously modify alkalinity, Ca availability, reaction products, and environmental performance.

The benefits of multicomponent complementarity are particularly evident in metallurgical and mixed industrial residues. A ternary ferronickel-slag/BFS/fly-ash system reached 69.6 MPa, while a GGBFS–EMR–OPC binder exceeded 8 MPa in sediment stabilization. A cement-free combination of oil-shale residue, steel slag, and soda residue reached 5.97 MPa as mine backfill and was associated with an estimated 86.9% reduction in CO_2 emissions [75,78,79]. In these systems, performance arose from the complementary supply of reactive silicate, Ca, alkali, sulfate, and other phase-forming species rather than from a single dominant component.

Hybrid matrices are especially useful when no individual waste supplies all required species. A calcined red-mud/GGBFS/phosphogypsum composition of 40/45/15 wt% exhibited lower porosity and water absorption and a 28 d strength 73.4% higher than that of the 70/15/15 mixture. An EMR/red-mud/GGBFS binder formed a sulfate- and alkali-regulated hybrid matrix with a flexural strength of approximately 6.6 MPa [55,56]. Here, red mud contributes Fe/Al-bearing phases and alkalinity, GGBFS supplies reactive Ca and silicate, and the sulfate-bearing component modifies early precipitation and hydration.

The effect of sulfate is therefore dosage- and phase-dependent. At controlled levels, sulfate promotes early AFt precipitation and can coexist with C-S-H/C-(A)-S-H and aluminosilicate gels, filling pores and densifying the hybrid matrix [55,56]. However, high sulfate availability can retard silicate hydration, while excessive or delayed ettringite/gypsum formation may generate crystallization stresses, microcracking, and loss of integrity. Thus, sulfate-bearing wastes should be optimized according to phase evolution rather than sulfate content alone, with long-term assessment of strength retention, dimensional stability, and sulfate resistance [55,56].

For backfill materials, matrix chemistry must be considered together with rheology and the stability of the surrounding environment. An EMR/coal-slag/BFS blend reached 19.3 MPa and remained stable in groundwater, NaCl, and Na_2SO_4 solutions, whereas red-mud/fly-ash/aeolian-sand backfill exhibited Herschel–Bulkley flow and 28 d strengths of 5.6–6.4 MPa depending on solids concentration [76,77].

Complementary mineral modules are also effective in geotechnical systems with relatively modest strength requirements. A GGBFS–EMR–OPC binder used for sediment stabilization exceeded 8 MPa while reducing the reported CO_2 burden and cost by 84.5% and 67%, respectively [78]. The oil-shale-residue/steel-slag/soda-residue system reached 5.97 MPa without cement or chemical additives and achieved the required backfill workability and leaching performance [79]. For road-subgrade stabilization, a full-solid-waste binder combining carbide slag, GGBFS, fly ash, silica fume, and desulfurization gypsum reached 6.88 MPa without external strong alkali [81].

A related waste-based stabilization strategy combined recycled demolition waste (RDW) with a GGBFS–fly-ash geopolymer binder for high-plasticity clay. Addition of 25% RDW increased the California bearing ratio (CBR) by 184%, while the combination of 25% RDW and 15% geopolymer binder increased unconfined compressive strength (UCS) approximately eightfold; XRD and SEM indicated that improved particle packing and geopolymeric bonding jointly contributed to densification and stabilization [85]. Other recent backfill studies likewise show that solids content, sulfate chemistry, activator dosage, bleeding, and setting behaviour are as important as peak strength [86–89].

The performance gains achieved in hybrid systems must also be compared with processing intensity. Alkali–thermal–mechanical treatment of EMR and vanadium-slag leach residue followed by the addition of 20% BFS yielded 23.8 MPa at 14 d and 35.1 MPa after autoclave drying [82]. In wet bauxite-residue/fly-ash/waste-glass geopolymers, increasing glass substitution improved scaling resistance but reduced structural strength; in a red-mud/waste-glass composite, the addition of 5% Portland cement increased strength by approximately 220% [83,84]. Such improvements may be technically useful, but the contribution of high-temperature processing, concentrated alkali, or clinker must remain visible in environmental comparisons.

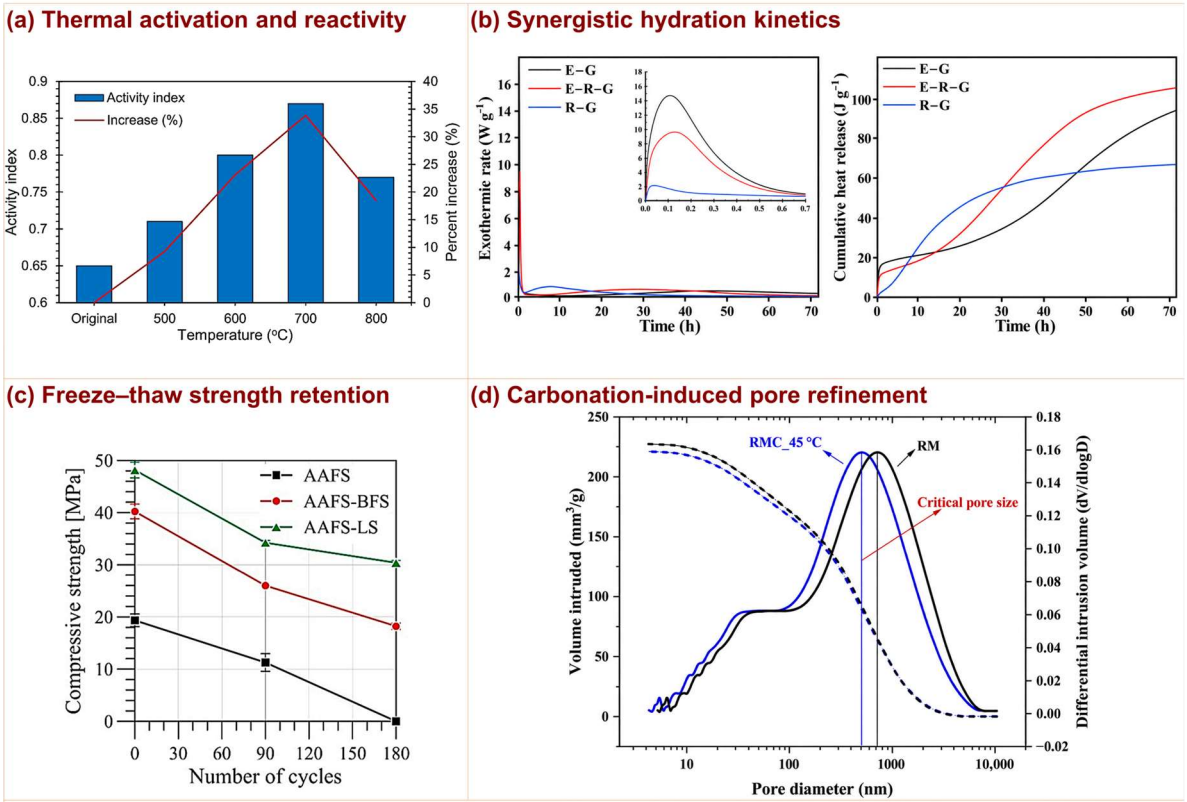
Low-temperature thermal modification of electrolytic manganese residue before incorporation into a GGBFS-based grout improved strength development and resistance to erosion under simulated service conditions [80]. This route is attractive because it uses a relatively mild pretreatment, although its technical benefit should still be evaluated against energy demand and the stability of residual Mn-bearing phases.

Alkali-thermal processing has also been used to incorporate up to 40 wt% red mud into one-part binders with a compressive strength of approximately 40 MPa [90]. Such routes reduce handling of liquid alkali at final mixing, but their practical value depends on storage stability, solid-activator dissolution, and sensitivity to water dosage and temperature. However, simplified water-only mixing does not eliminate field-scale risks in one-part systems. Pre-blended alkali-activated binders can undergo storage-induced changes, particularly under exposure to ambient moisture, which may alter subsequent hydration kinetics and early strength development [91]. In addition, incomplete dissolution of granular solid activators and excessively rapid setting can compromise mixture homogeneity and workability [92], while mixing-water temperature can substantially modify solid-activator dissolution, slump retention, and setting behaviour under realistic hot- or cold-weather conditions [93]. For waste-derived systems, these operational sensitivities are compounded by batch-to-batch mineralogical variability, which can change precursor reactivity and the response to a nominally identical activation treatment [52]. Large-scale application therefore requires moisture-controlled storage and shelf-life testing of dry blends, batch-specific mineralogical and chemical quality control, verification of solid-activator dissolution and dry-blend homogeneity, and robustness testing across realistic variations in water dosage, mixing temperature, and ambient conditions.

Additive-assisted modification has also been demonstrated for steel-slag geopolymers containing recycled wind-turbine-blade powder. Glass-fibre-reinforced polymer and balsawood fractions contributed to stress transfer, crack suppression, and enhanced hydration, with 6 wt% WTB-WB providing the reported optimum balance between reduced density and physical performance [94].

Figure 4 integrates representative phase-transformation and performance responses across different levels of mineralogical utilization and compensation. Figure 4a shows that calcination increased the red-mud activity index from approximately 0.66 in the original state to about 0.88 at 700 °C, followed by a decline to about 0.78 at 800 °C, demonstrating that over-calcination can reduce rather than increase reactivity [56]. Figure 4b illustrates synergistic hydration in an EMR/red-mud/GGBFS binder: The sulfate- and alkali-bearing combination generated a distinct secondary exothermic feature and greater cumulative heat release over 72 h, consistent with prolonged reaction and hybrid-product formation [55]. Figure 4c demonstrates the service consequence of chemical complementarity. Pure alkali-activated fayalite slag failed after 180 freeze–thaw cycles, whereas BFS- and ladle-slag-modified compositions retained approximately 20 and 30 MPa, respectively [68]. Figure 4d shows that carbonation of red mud at 10 bar CO_2 and 45 °C reduced the critical pore diameter from 720 to 510 nm and porosity from 54.4 to 34.5%, even though the measured

uptake was only 2.7 g CO_2 per 100 g of red mud [22]. These cases show that phase transformation and pore-structure control affect application-relevant performance. Service-specific validation should also include parameters such as hydraulic conductivity and environmental compliance where relevant [95,96].



Note: Panels represent independent studies and are intended for qualitative comparison only; direct numerical comparison across panels is not appropriate.

Figure 4. Representative activation–structure–performance relationships across self-sufficient, binary, and multicomponent waste-derived systems: (**a**) thermal activation and reactivity [56], (**b**) synergistic hydration kinetics [55], (**c**) freeze–thaw strength retention [68] and (**d**) carbonation-induced pore refinement [22] (In (**d**), dashed lines represent the cumulative intruded volume, while solid lines represent the differential intrusion curves; black and blue lines correspond to RM and RMC_45 °C, respectively). The panels represent independent case studies and are not intended for direct quantitative comparison. Adapted from Refs. [22,55,56,68] with permission.

Long-term contaminant retention is controlled by both the mineral hosts in the precursor and the stability of the reaction products formed during activation. N-A-S-H-type aluminosilicate matrices can contribute to retention through charge-balancing sites and physical encapsulation, whereas Ca-bearing C-(A)-S-H-type products provide additional sorption or incorporation environments and can restrict contaminant transport through pore refinement [97,98]. Fe- and Al-bearing oxide or hydroxide phases may provide additional surface-sorption and co-precipitation sites, while sulfate-bearing systems can modify element partitioning through AFt-type phase formation [7,23,24]. These mechanisms are conditional rather than permanent: Acidification and carbonation can destabilize Ca-bearing hydrates or sulfate-containing phases, whereas redox-driven transformation of Fe- or sulfide-bearing phases can increase trace-element mobility [6,53,99]. Immobilization should therefore be interpreted as a mineralogical phase-stability problem rather than inferred solely from low initial leachate concentrations.

For contaminant-bearing waste-derived AAMs, short-term compliance leaching tests should therefore be complemented by long-term exposure protocols that reproduce changes expected under service conditions. Validation should include monolithic rather than only crushed-sample leaching, repeated or sequential sampling, and exposure to acidic, near-neutral, and alkaline conditions. Carbonation should be evaluated before or during leaching because the associated decrease in alkalinity and phase transformation may alter contaminant retention, while sulfide- or Fe-bearing wastes should additionally be tested under alternating oxidizing and reducing conditions because redox-driven phase transformations can modify trace-element mobility [6,47,53,99]. Persistent immobilization should be assessed from cumulative contaminant release together with solution pH and redox potential, permeability, mass and strength retention, and post-exposure mineralogical or microstructural changes rather than from a single short-duration extraction test.

The evidence reviewed above indicates that the need for additional precursors is governed by the mineralogical sufficiency of the original waste rather than by its industrial origin or bulk oxide composition. Binary systems compensate for a dominant limitation through one additional mineral component, whereas multicomponent systems distribute matrix-forming, activating, and stabilizing functions among several complementary solids. Increasing formulation complexity is therefore justified only when it produces a demonstrable gain in phase accessibility, reaction-product development, durability, environmental stability, or application-specific performance.

Neither high compressive strength nor a high waste fraction is sufficient to demonstrate chemical participation or environmental benefit. Pretreatment routes involve different energy–reagent trade-offs. Thermal activation can efficiently dehydroxylate or amorphize resistant phases but introduces a direct heat demand [20,21,52], whereas hydrothermal activation may substantially increase precursor dissolution but combines elevated temperature and pressure with concentrated alkali consumption [57]. Mechanochemical activation avoids bulk heating and can reduce chemical demand, although prolonged grinding introduces an electrical-energy penalty and may show diminishing returns [67,72]. Direct alkaline activation generally requires less thermal pretreatment but transfers part of the environmental burden to NaOH or sodium-silicate production, whereas waste-derived activators or chemically complementary co-precursors can reduce commercial-reagent demand [26,63]. Processing routes should therefore be compared within consistent system boundaries that include pretreatment energy, activator production and dosage, co-binder content, achieved reactivity and strength, durability, leaching, and, where available, cost and life-cycle indicators [100–103]. Performance criteria should remain application-specific: mine backfill and subgrade materials require reliable rheology, early stability, and leaching control; structural products require long-term mechanical and durability validation; and porous products require a controlled balance among density, strength, thermal conductivity, and moisture resistance. The preferred route is therefore not necessarily the one producing maximum reactivity, but the least intensive treatment that reliably satisfies the requirements of the intended application. Economic comparisons should likewise be normalized to a functional unit, such as the cost per tonne of qualified material or per unit of product meeting specified strength, durability, and leaching requirements, rather than considering binder cost alone.

Although laboratory studies still dominate the literature, several waste-derived systems have progressed to pilot-scale production and field implementation. Lu et al. developed an alkali-activated road material from open-pit mine road aggregate, GGBFS, and coal fly ash and subsequently validated the optimized formulation through construction of an actual haul-road section at an open-pit coal mine [104]. Qin et al. similarly converted coal slurry, slag powder, and fly ash into a geopolymer pavement material and demonstrated

its engineering application in a coal-mine pavement [105]. In the metallurgical-waste sector, Kriskova et al. transferred bauxite-residue- and steel-slag-based formulations from laboratory optimization to pilot-scale production and outdoor demonstration, including 250 m^2 of bauxite-residue pavement and 20 m^2 of steel-slag pavers [106]. Longer-term field evidence is provided by high-density geopolymer concrete containing steel-furnace-slag aggregate and a GGBFS–fly-ash binder, with approximately 90 m^3 installed as breakwater armour units and evaluated after three years of marine exposure [107]. These examples demonstrate that mining- and metallurgical-waste-derived materials can progress beyond laboratory formulation; however, such evidence remains limited relative to the laboratory literature and is concentrated in a small number of waste streams and applications.

4. Artificial Intelligence and Machine Learning for Predictive Materials Design

Despite substantial progress in understanding the mineralogical and chemical regularities of waste conversion, practical formulation of geopolymeric and alkali-activated materials remains difficult. Multicomponent compositions, feedstock variability, and nonlinear structure development make conventional empirical optimization labour-intensive and often poorly transferable. Artificial intelligence and machine learning (AI and ML) can accelerate property prediction, identify hidden relationships among precursor characteristics, activation parameters, and final performance, and guide the selection of subsequent experiments. They should, however, complement rather than replace mineralogical characterization and experimental validation.

Compressive-strength prediction remains the most developed application. Early studies used artificial neural networks and optimized support-vector-machine models to predict the strength of alkali-activated slags and related binders [108,109]. Later work on fly-ash geopolymer concrete demonstrated that nonlinear algorithms could outperform conventional regression when mixture proportions and curing conditions were included [110]. In one comparison, extreme gradient boosting (XGBoost) reached $R^2 = 0.98$, whereas SVM and multilayer perceptron models achieved R^2 values of 0.91 and 0.88; the corresponding best-model errors were MAE = 1.49 MPa and RMSE = 1.78 MPa [111]. Such metrics are encouraging, but they are meaningful only when the validation design prevents information leakage between closely related mixtures.

The scope of ML has expanded from single-system prediction to broader datasets and multi-algorithm comparisons [112–114]. In an experimental study covering four industrial-waste streams—blast-furnace slag, fly ash, reducing slag, and waste glass—42 mixtures were used to train and compare models. A random-forest model was selected for optimization, and the subsequently tested composition increased compressive strength by 59.65% relative to the reference mixture [115]. The value of this workflow lies not only in prediction, but in closing the loop between model recommendation and experimental verification.

High coefficients of determination obtained from randomly split datasets can nevertheless overstate generalization. Samples from the same experimental campaign often share precursor batches, activator chemistry, and curing conditions; distributing them between training and test sets makes the prediction task artificially easy. Study-level or precursor-batch-grouped validation is therefore preferable when the aim is to predict new wastes. Applicability domains and predictive uncertainty should also be reported so that extrapolation beyond the training data can be identified explicitly.

A central limitation of current databases is the sparse description of precursor mineralogy. Most models use mass fractions, water/binder ratio, activator dosage, curing time, and temperature, while phase assemblage, amorphous content, particle size, and dissolution behaviour are rarely included. A chemistry-informed analysis of 676 geopolymer

compositions showed that incorporating compositional descriptors can improve the interpretation of strength development [116]. Coupling machine learning with thermodynamic information provides a further route for constraining predictions by physically plausible reaction products [117].

Bulk SiO_2, Al_2O_3, CaO, and Fe_2O_3 contents are only indirect proxies for reactivity. The same SiO_2 content may represent inert quartz in one tailings sample and reactive glass in another. Likewise, Fe-, Ca-, Mg-, Al-, and sulfate-bearing wastes must be described according to the actual mineral hosts—such as crystalline oxides, hydroxides, carbonates, sulfates, or amorphous phases—because bulk oxide totals do not distinguish reactive from inert or poorly accessible forms. Models based solely on oxide totals may fit a restricted dataset yet fail for a new residue with different mineral hosts [118]. Future datasets should therefore include quantitative phase composition, amorphous fraction, specific surface area, particle-size distribution, and standardized dissolution indicators.

Explainable artificial intelligence can help determine whether a model has learned chemically plausible relationships. XGBoost combined with SHapley Additive exPlanations (SHAP) analysis has been used to interpret strength development in one-part dry alkali-activated materials [119], while interpretable models have also been applied to slump and compressive strength in fly-ash geopolymer concrete [120]. SHAP values and related importance measures identify statistical contributions rather than causal mechanisms [119,120]. Their mechanistic interpretation should therefore be validated experimentally: phase- or amorphous-content effects by quantitative XRD and reaction-product analysis [40–42], kinetic effects by calorimetry, and inferred precursor reactivity by standardized dissolution measurements [43]. Agreement among independent mineralogical and physicochemical measurements should be established before statistical feature importance is interpreted as evidence of a reaction mechanism [116,117].

Beyond forward prediction, ML supports inverse design: selecting compositions that satisfy specified strength, cost, and environmental objectives. Random-forest-based optimization has been used for alkali-activated concrete formulations [121], and multi-objective frameworks have jointly considered compressive strength, cost, and CO_2 emissions [122]. Soft-computing approaches provide another means of exploring trade-offs among competing performance targets [123]. For waste-derived materials, batch-to-batch variability should be represented explicitly through measured ranges or probability distributions of mineralogical descriptors, including quantitative phase contents, amorphous fraction, and dissolution-related variables [116–118]. Inverse-design optimisation should then identify formulations that satisfy performance, leaching, and durability requirements across these plausible precursor compositions rather than for a single nominal batch [121–123]. Precursor-batch-grouped validation, prediction uncertainty, and applicability-domain checks should be used to reject solutions that rely on extrapolation beyond the characterized feedstock range. Activator availability and curing-energy constraints should be included simultaneously in the optimisation.

The most useful workflow is iterative: model, experiment, update, and repeat [124]. Active or sequential learning is particularly suitable for highly variable wastes because the algorithm selects the next experiment that is expected to provide the greatest information gain or improvement toward the target. In a study based on 284 records and 18 input variables, the model achieved an accuracy of 98.9%, corresponding to an improvement of 4.1% over the baseline approach [125]. Such results should nevertheless be interpreted together with dataset size, validation strategy, and the definition of the reported accuracy metric.

Durability prediction is developing more slowly than strength prediction because exposure tests are longer, protocols are less uniform, and failure mechanisms are more complex. ML has been applied to the high-temperature response of geopolymer concrete [126]

and to freeze–thaw performance in one-part geopolymer-stabilized soil [127]. Broader attempts to predict durability and environmental performance remain limited [128]. Progress requires datasets that record not only mixture design, but exposure solution, cycle definition, specimen geometry, preconditioning, mass change, strength retention, permeability, and leaching.

For the framework proposed in this review, model variables can be organized into three categories—precursor descriptors, processing and activation variables, and reaction-product descriptors—while application-performance metrics are treated as prediction targets. Precursor descriptors include quantitative phase composition, amorphous content, particle size, specific surface area, and dissolution indices. Processing variables include grinding energy, calcination or hydrothermal conditions, activator chemistry and dosage, liquid-to-solid ratio, curing regime, and co-precursor content. Reaction-product descriptors, such as gel or hydrate assemblage and pore structure, may serve as intermediate mechanistic features, whereas strength, thermal conductivity, durability, leaching, and CO_2-related indicators should be treated as target variables according to the modelling objective.

For transferable modelling, precursor descriptors should represent the mineralogical functions relevant to the reaction rather than predefined waste classes. Minimum inputs should therefore include quantitative contents of major crystalline and amorphous phases, amorphous fraction, standardized soluble or accessible Si and Al, reactive Ca/Mg-bearing phases, Fe and Al speciation where relevant, sulfate and carbonate phase contents, alkalinity or carbonation potential, specific surface area, and particle-size descriptors [31,32,40–42]. For compensated systems, the mineralogical contribution and dosage of each functional co-precursor should be recorded explicitly. Processing variables—including activator chemistry and dosage, liquid-to-solid ratio, grinding, thermal or hydrothermal pretreatment, and curing regime—should then be coupled with these precursor descriptors. Recent chemistry- and physics-informed ML frameworks further support the use of physically meaningful mineralogical and mechanistic variables rather than conventional mixture proportions or bulk oxide composition alone [129,130].

AI and ML can therefore support a transition from trial-and-error formulation to predictive materials design, but the most robust strategy is a hybrid one: mineralogical characterization to define physically meaningful inputs; interpretable ML for screening and optimization; thermodynamic or kinetic constraints to restrict implausible predictions; uncertainty quantification to identify extrapolation; and targeted experiments to validate the selected formulations. Without this integration, a high statistical score may conceal a model that is accurate only within a narrow and poorly transferable dataset.

Improving model transferability will also require coordinated data generation rather than isolated single-laboratory datasets. A shared machine-readable reporting schema should be adopted for waste-derived AAMs, together with multi-institutional benchmark datasets covering geographically and mineralogically distinct waste sources. Interlaboratory studies using common mineralogical characterization, dissolution, curing, durability, and leaching protocols would allow models to be externally validated across precursor batches and regions. Open repositories should retain batch identifiers, measurement uncertainty, processing metadata, and unsuccessful as well as successful formulations to reduce publication bias and define realistic applicability domains.

5. Conclusions

This review synthesized current approaches for converting mining, metallurgical, and mixed industrial wastes into geopolymeric, alkali-activated, and related mineral matrices. The central conclusion is that waste suitability is determined not by its industrial name or bulk contents of SiO_2, Al_2O_3, CaO, Fe_2O_3 and MgO, but by the mineral forms in which

these components occur, their solubility and accessibility, and their reaction roles within the overall formulation.

The primary design distinction is whether the intrinsic mineral inventory of a waste is sufficient for the intended transformation. In self-sufficient systems, processing should maximize the accessibility and reaction of intrinsic phases through dissolution, amorphization, dehydroxylation, mechanochemical activation, carbonation, or related transformations. Where the intrinsic inventory is insufficient, additional mineral solids should be selected according to the missing functional contribution—such as reactive Si/Al, Ca, sulfate, alkalinity, or complementary phase-forming capacity. Binary compensation can address a dominant limitation through one additional functional solid, whereas multicomponent formulations distribute several complementary functions among multiple precursors. Formulation complexity is therefore justified only when it produces a demonstrable improvement in reaction-product development, durability, environmental stability, or application-specific performance.

The required product form should determine the activation strategy. Mine backfill and subgrade materials may tolerate moderate strength but require reliable rheology, early stability, leaching control, and low processing cost. Structural products require sustained strength and durability under relevant exposure conditions. Porous thermal-insulation materials require controlled cell architecture rather than maximum porosity. Carbonation and CO_2 mineralization can improve pore structure and bind carbon in Ca- and Mg-bearing wastes, but their benefit depends on reaction extent, permanence, and the energy and pressure required.

The principal obstacles to scale-up are feedstock variability, intensive pretreatment, activator-related environmental impacts, and insufficient durability and leaching data. Results should be compared only across compatible formulations, specimen geometries, curing regimes, and test methods. A high waste fraction or compressive strength does not prove that the waste has reacted chemically; quantitative phase analysis, dissolution measurements, and reaction-product identification are required to distinguish a reactive precursor from a filler.

Machine learning can accelerate mixture screening and inverse design, but its reliability is constrained by data quality. Future databases should include quantitative phase composition, amorphous fraction, particle-size distribution, dissolution behaviour, activator chemistry, curing energy, environmental indicators, and uncertainty. Interpretable and physics-informed models, combined with grouped validation and targeted experiments, are more likely to transfer across waste sources than black-box models trained only on mixture proportions and bulk oxide contents.

The highest-priority gaps for industrial deployment are therefore twofold. Experimentally, future work should prioritize validation across representative waste batches, scale-appropriate processing and ambient curing, long-term durability and contaminant retention, and integrated assessment of mechanical performance, leaching, energy and reagent demand, cost, and life-cycle impacts. From a data-development perspective, transferable databases should record batch-resolved quantitative mineralogy, amorphous fraction, particle-size distribution, standardized dissolution or reactivity indicators, activation and curing conditions, reaction-product assemblage, durability and leaching outcomes, validation scale, and associated uncertainty. Addressing these experimental and data gaps together is essential for moving mineralogy-guided waste valorization from laboratory optimization toward reproducible industrial deployment.

https://doi.org/10.3390/min16090936

Author Contributions: Conceptualization, A.I., G.S. and V.E.; methodology, A.I., K.K. and A.K.; validation, G.S., V.E., L.M. and A.B.; formal analysis, A.I., K.K. and A.Z.; investigation, A.I., V.E., L.M., A.B., R.A., A.Z. and A.K.; resources, G.S., K.K. and R.A.; data curation, A.I., L.M., A.B. and A.Z.; writing—original draft preparation, A.I. and V.E.; writing—review and editing, G.S., V.E., K.K., L.M., A.B., R.A., A.Z. and A.K.; visualization, A.I., L.M. and A.Z.; supervision, G.S., V.E. and K.K.; project administration, G.S. and R.A.; funding acquisition, G.S. and R.A. All authors have read and agreed to the published version of the manuscript.

Funding: This research was funded by the Science Committee of the Ministry of Science and Higher Education of the Republic of Kazakhstan, grant number BR28712667.

Data Availability Statement: No new data were created or analyzed in this study. Data sharing is not applicable to this article.

Conflicts of Interest: The authors declare no conflicts of interest.

Abbreviations

AAM	Alkali-activated material
BFS	Blast-furnace slag
C-(A)-S-H	Calcium (alumino)silicate hydrate
C-(N)-A-S-H	Calcium-(sodium) aluminosilicate hydrate
C-S-H	Calcium silicate hydrate
CCS	Calcium carbide slag
CSD	Calcium sulfate dihydrate
EMR	Electrolytic manganese residue
FA	Fly ash
GGBFS	Ground-granulated blast-furnace slag
L/S	Liquid-to-solid ratio
MK	Metakaolin
ML	Machine learning
N-A-S-H	Sodium aluminosilicate hydrate
N-(C)-A-S-H	Sodium-(calcium) aluminosilicate hydrate
OPC	Ordinary Portland cement
PG	Phosphogypsum
PC	Portland cement
RM	Red mud
UCS	Unconfined compressive strength

References

1. Verma, H.; Mishra, P.N.; Manna, B.; Williams, D. Critical Appraisal of Characterization, Valorization, and Management Pathways of Mine Wastes. *J. Hazard. Toxic Radioact. Waste* **2026**, *30*, 03126002. [CrossRef]
2. Dassanayake, C.; Mashaan, N.S.; Oguntayo, D. Mining Waste as a Resource in Construction: Applications, Benefits, and Challenges. *Sustainability* **2026**, *18*, 1361. [CrossRef]
3. Li, T.; Desta, F.; Buxton, M. Recent Advancements in Digital Management and Monitoring of Mine Waste: Sensors, Characterization, and Predictive Modeling—A Review. *Sensors* **2026**, *26*, 3553. [CrossRef]
4. Adesina, A. Synthesis, Characterization, and Efficacy of Alkali-Activated Materials from Mine Tailings: A Review. *Waste Manag.* **2025**, *191*, 23–46. [CrossRef]
5. Arancibia-Zúñiga, A.; Carlesi, C.; Chamy, R.; Morales, J. Valorization of Copper Slag Through Alkali-Activated Materials: A Systematic Review. *Sustainability* **2026**, *18*, 4924. [CrossRef]
6. Gan, C.; Yang, J.; Li, J.; Du, X.; Huang, J.-H.; Wang, X.; Shaheen, S.M.; Rinklebe, J. Iron (Hydr)Oxides and Oxalic Acid Drive Vanadium Transformation in Mine Tailings under Repeated Redox Fluctuations. *Environ. Sci. Technol.* **2025**, *59*, 26133–26144. [CrossRef]
7. Durocher, J.L.; Schindler, M. Iron-Hydroxide, Iron-Sulfate and Hydrous-Silica Coatings in Acid-Mine Tailings Facilities: A Comparative Study of Their Trace-Element Composition. *Appl. Geochem.* **2011**, *26*, 1337–1352. [CrossRef]

8. Rodríguez-Pacheco, R.; García, G.; Caparrós-Ríos, A.V.; Robles-Arenas, V.; García-García, C.; Millán, R.; Pérez-Sanz, A.; Alcolea-Rubio, L.A. Mineralogy, Geochemistry and Environmental Hazards of Different Types of Mining Waste from a Former Mediterranean Metal Mining Area. *Land* **2023**, *12*, 499. [CrossRef]
9. Chen, W.; Zhu, H.; Li, Y.; Liu, F.; Li, Q.; Mao, Y.; Yang, A. Geopolymers Prepared from Industrial Solid Waste: Comprehensive Properties and Application Prospects. *Environ. Res.* **2025**, *278*, 121518. [CrossRef]
10. Habert, G.; d'Espinose De Lacaillerie, J.B.; Roussel, N. An Environmental Evaluation of Geopolymer Based Concrete Production: Reviewing Current Research Trends. *J. Clean. Prod.* **2011**, *19*, 1229–1238. [CrossRef]
11. McLellan, B.C.; Williams, R.P.; Lay, J.; Van Riessen, A.; Corder, G.D. Costs and Carbon Emissions for Geopolymer Pastes in Comparison to Ordinary Portland Cement. *J. Clean. Prod.* **2011**, *19*, 1080–1090. [CrossRef]
12. Turner, L.K.; Collins, F.G. Carbon Dioxide Equivalent (CO_2-e) Emissions: A Comparison between Geopolymer and OPC Cement Concrete. *Constr. Build. Mater.* **2013**, *43*, 125–130. [CrossRef]
13. Piovesan, M.A.; Bruschi, G.J.; Kubiaki Levandoski, W.M.; Fante, F.; Korf, E.P. Recent Advances in the Alkali-Activated Stabilization of Zinc Mine Tailings. *Constr. Mater.* **2026**, *6*, 39. [CrossRef]
14. Maali, A.; Mohamedelhassan, E.; Bediwy, A. Utilization of Mine Tailings in Concrete Production: A Bibliometric and Technical Review of Challenges, Potential, and Innovation Pathways. *Mater. Today Sustain.* **2026**, *34*, 101325. [CrossRef]
15. Maali, A.; Bediwy, A.; Mohamedelhassan, E. Gold Mine Tailings in Concrete and SCMs: Comprehensive Review of Reactivity Enhancement, Optimized Performance, and Pathways to Sustainability. *Mater. Today Adv.* **2026**, *29*, 100688. [CrossRef]
16. Raja, R.; Kumar, S.; Kirchheim, A.P. Beyond Waste: Performance Insights into Non-Ferrous Slag-Based Cementitious Composites—A Review. *J. Build. Rehabil.* **2026**, *11*, 169. [CrossRef]
17. Li, Z.; Yuan, X.; Fu, H.; Lin, S.; Xu, X. Microbially Induced Mineralization for Mine Tailings Treatment: Progress, Challenges, and Future Prospects. *J. Environ. Manag.* **2026**, *413*, 130350. [CrossRef]
18. Provis, J.L. Alkali-Activated Materials. *Cem. Concr. Res.* **2018**, *114*, 40–48. [CrossRef]
19. Liu, H.; Zhang, Y.; Chen, C.; Huang, Y.; Chen, Z. Research on Leaching Kinetics and Reactivity Evaluation of Copper Tailings as Precursor for Alkali-Activated Materials. *Case Stud. Constr. Mater.* **2024**, *21*, e03663. [CrossRef]
20. Luo, X.; Huang, L.; Li, Y.; Chen, Z. Preparation of Geopolymers from Thermally Activated Lithium Slag as Sole Precursor: Mechanical Properties and Microstructure. *Case Stud. Constr. Mater.* **2024**, *20*, e03248. [CrossRef]
21. Meilasari, F.; Trihadiningrum, Y.; Warmadewanthi, I.D.A.A.; Sutrisno, H.; Ekaputri, J.J. Valorization of Bauxite Residue for Sustainable Construction Materials: Chemical, Thermal, and Mechanical Properties. *Clean. Waste Syst.* **2025**, *12*, 100343. [CrossRef]
22. Duraisamy, S.; Chaunsali, P. Stabilization of Red Mud Using Mineral Carbonation. *Clean. Eng. Technol.* **2025**, *25*, 100926. [CrossRef]
23. Xing, Y.; Wang, B.; Yu, H. Effect of Alkali-Activation Conditions on Microstructure and Heavy Metal Solidification of Alkali-Activated Converter Steel Slag and Municipal Solid Waste Incineration Fly Ash. *Environ. Res.* **2025**, *267*, 120654. [CrossRef]
24. Xing, Y.; Wang, B. Modification of Phases Evolution and Heavy Metal Immobilization in Alkali-Activated MSWI FA by the Incorporation of Converter Steel Slag. *J. Build. Eng.* **2023**, *78*, 107573. [CrossRef]
25. Najafi, E.K.; Miranda, T.; Unluer, C.; Pourakbar, S.; Manaviparast, H.R.; Tavares, P.; Cristelo, N. Sustainable Alkaline Cements with Different Ca Contents for Stabilisation of Copper Mine Tailings. *J. Clean. Prod.* **2026**, *538*, 147411. [CrossRef]
26. Duan, S.; Li, Y.; Li, X.; Wu, H.; Lu, G.; Guo, Y.; Ma, Z. Performance and Mechanisms of Calcium Carbide Slag as a Low-Cost Alkaline Activator for Sustainable Fly Ash-Red Mud Geopolymers. *Case Stud. Constr. Mater.* **2026**, *24*, e06133. [CrossRef]
27. Provis, J.L.; Palomo, A.; Shi, C. Advances in Understanding Alkali-Activated Materials. *Cem. Concr. Res.* **2015**, *78*, 110–125. [CrossRef]
28. Xiao, R.; Jiang, X.; Zhang, M.; Polaczyk, P.; Huang, B. Analytical Investigation of Phase Assemblages of Alkali-Activated Materials in CaO-SiO_2-Al_2O_3 Systems: The Management of Reaction Products and Designing of Precursors. *Mater. Des.* **2020**, *194*, 108975. [CrossRef]
29. Yu, X.; Shi, J.; He, Z.; Yalçınkaya, Ç.; Revilla-Cuesta, V.; Gencel, O. Review of the Materials Composition and Performance Evolution of Green Alkali-Activated Cementitious Materials. *Clean Technol. Environ. Policy* **2023**, *25*, 1439–1459. [CrossRef]
30. He, X.; Yuhua, Z.; Qaidi, S.; Isleem, H.F.; Zaid, O.; Althoey, F.; Ahmad, J. Mine Tailings-Based Geopolymers: A Comprehensive Review. *Ceram. Int.* **2022**, *48*, 24192–24212. [CrossRef]
31. Ponomar, V.; Yliniemi, J.; Adesanya, E.; Ohenoja, K.; Illikainen, M. An Overview of the Utilisation of Fe-Rich Residues in Alkali-Activated Binders: Mechanical Properties and State of Iron. *J. Clean. Prod.* **2022**, *330*, 129900. [CrossRef]
32. Peys, A.; Isteri, V.; Yliniemi, J.; Yorkshire, A.S.; Lemougna, P.N.; Utton, C.; Provis, J.L.; Snellings, R.; Hanein, T. Sustainable Iron-Rich Cements: Raw Material Sources and Binder Types. *Cem. Concr. Res.* **2022**, *157*, 106834. [CrossRef]
33. Luo, X.; Tian, X.; Wu, J.; Yang, X.; Liu, Z.; Jiao, Z.; Peng, H. Molecular Simulations of the Initial Stage's Induction and Formation Process of N-A-S-H Gel Based on NaOH-Activated Metakaolin. *J. Non-Cryst. Solids* **2024**, *626*, 122804. [CrossRef]
34. Garcia-Lodeiro, I.; Palomo, A.; Fernández-Jiménez, A.; Macphee, D.E. Compatibility Studies between N-A-S-H and C-A-S-H Gels. Study in the Ternary Diagram Na_2O–CaO–Al_2O_3–SiO_2–H_2O. *Cem. Concr. Res.* **2011**, *41*, 923–931. [CrossRef]

35. Walkley, B.; San Nicolas, R.; Sani, M.-A.; Rees, G.J.; Hanna, J.V.; Van Deventer, J.S.J.; Provis, J.L. Phase Evolution of C-(N)-A-S-H/N-A-S-H Gel Blends Investigated via Alkali-Activation of Synthetic Calcium Aluminosilicate Precursors. *Cem. Concr. Res.* **2016**, *89*, 120–135. [CrossRef]
36. Bernal, S.A.; Provis, J.L.; Walkley, B.; San Nicolas, R.; Gehman, J.D.; Brice, D.G.; Kilcullen, A.R.; Duxson, P.; Van Deventer, J.S.J. Gel Nanostructure in Alkali-Activated Binders Based on Slag and Fly Ash, and Effects of Accelerated Carbonation. *Cem. Concr. Res.* **2013**, *53*, 127–144. [CrossRef]
37. Lothenbach, B.; Scrivener, K.; Hooton, R.D. Supplementary Cementitious Materials. *Cem. Concr. Res.* **2011**, *41*, 1244–1256. [CrossRef]
38. Provis, J.L.; Bernal, S.A. Geopolymers and Related Alkali-Activated Materials. *Annu. Rev. Mater. Res.* **2014**, *44*, 299–327. [CrossRef]
39. Makole, K.M.; Horn, E.J.; Randall, D.G. Geopolymerization: A Novel Method for Manufacturing Tiles from Copper Mine Tailings. *Results Eng.* **2026**, *30*, 111040. [CrossRef]
40. Obenaus-Emler, R.; Falah, M.; Illikainen, M. Assessment of Mine Tailings as Precursors for Alkali-Activated Materials for on-Site Applications. *Constr. Build. Mater.* **2020**, *246*, 118470. [CrossRef]
41. Bhagath Singh, G.V.P.; Subramaniam, K.V.L. Quantitative XRD Study of Amorphous Phase in Alkali Activated Low Calcium Siliceous Fly Ash. *Constr. Build. Mater.* **2016**, *124*, 139–147. [CrossRef]
42. Snellings, R.; Salze, A.; Scrivener, K.L. Use of X-Ray Diffraction to Quantify Amorphous Supplementary Cementitious Materials in Anhydrous and Hydrated Blended Cements. *Cem. Concr. Res.* **2014**, *64*, 89–98. [CrossRef]
43. Panagiotopoulou, C.; Kontori, E.; Perraki, T.; Kakali, G. Dissolution of Aluminosilicate Minerals and By-Products in Alkaline Media. *J. Mater. Sci.* **2007**, *42*, 2967–2973. [CrossRef]
44. Komnitsas, K.; Zaharaki, D. Geopolymerisation: A Review and Prospects for the Minerals Industry. *Miner. Eng.* **2007**, *20*, 1261–1277. [CrossRef]
45. Chen, Y.; Tong, X.; Kang, X. Particle-Chain Structure Induced by GO/MXenes Enhances High Iron Ore Tailings Content-Based Alkali Activated Geopolymer Unburned Bricks. *J. Build. Eng.* **2026**, *127*, 116411. [CrossRef]
46. Ahmari, S.; Zhang, L. Production of Eco-Friendly Bricks from Copper Mine Tailings through Geopolymerization. *Constr. Build. Mater.* **2012**, *29*, 323–331. [CrossRef]
47. Ahmari, S.; Zhang, L. Durability and Leaching Behavior of Mine Tailings-Based Geopolymer Bricks. *Constr. Build. Mater.* **2013**, *44*, 743–750. [CrossRef]
48. Navarro, R.; Alcocel, E.G.; Garcés, P.; Sánchez, I.; Zornoza, E. Characterization of Alkali Activated SiMn Slag Paste with Carbon Fibre as Heating Material for Building Applications. *Constr. Build. Mater.* **2026**, *520*, 146050. [CrossRef]
49. Sanna, A.; Uibu, M.; Caramanna, G.; Kuusik, R.; Maroto-Valer, M.M. A Review of Mineral Carbonation Technologies to Sequester CO_2. *Chem. Soc. Rev.* **2014**, *43*, 8049–8080. [CrossRef]
50. Bobicki, E.R.; Liu, Q.; Xu, Z.; Zeng, H. Carbon Capture and Storage Using Alkaline Industrial Wastes. *Prog. Energy Combust. Sci.* **2012**, *38*, 302–320. [CrossRef]
51. Tileuberdi, Y.; Imanbayev, Y.; Kanzharkan, Y.; Kidyrali, A.; Frolov, S.; Bektenov, N. Identification and Characterization of Sulfur Cake from Stepnogorsk Sulfuric Acid Plant. *Eurasian Chem. Technol. J.* **2024**, *26*, 265–271. [CrossRef]
52. Liu, J.; Doh, J.-H.; Ong, D.E.L.; Kiely, F.L. Effect of Thermal Pretreatment on the Reactivity of Red Mud Valorized as Aluminosilicate Precursor for Geopolymer Production. *Constr. Build. Mater.* **2024**, *445*, 137943. [CrossRef]
53. Zhang, M.; Zhao, M.; Zhang, G.; Mann, D.; Lumsden, K.; Tao, M. Durability of Red Mud-Fly Ash Based Geopolymer and Leaching Behavior of Heavy Metals in Sulfuric Acid Solutions and Deionized Water. *Constr. Build. Mater.* **2016**, *124*, 373–382. [CrossRef]
54. Konduru, H.; Karthiyaini, S. Enhancing Solidification in One-Part Geopolymer Systems through Alkali-Thermal Activation of Bauxite Residue and Silica Fume Integration. *Case Stud. Constr. Mater.* **2024**, *21*, e03444. [CrossRef]
55. Jiang, X.; Wang, L.; Zhang, W.; Li, Z.; Li, Y. Synergistic Mechanism of Electrolytic Manganese Residue and Red Mud in Ground Granulated Blast Furnace Slag-Based Cementitious Materials System: Multiscale Analysis Based on Hydration Characteristics and Mechanical Properties. *Case Stud. Constr. Mater.* **2025**, *23*, e05320. [CrossRef]
56. Raza, A.; Selmi, A.; Elhadi, K.M.; Ghazouani, N.; Chen, W. Strength Analysis and Microstructural Characterization of Calcined Red Mud Based-Geopolymer Concrete Modified with Slag and Phosphogypsum. *J. Mater. Res. Technol.* **2024**, *33*, 6168–6181. [CrossRef]
57. Yang, Y.; Zhang, J.; Fu, Y.; Hou, D.; Dong, B. Alkaline Hydrothermal Activation of Molybdenum Tailings to Prepare One-Part Geopolymer: Activation Mechanism and Strength. *J. Mater. Res. Technol.* **2023**, *25*, 3789–3802. [CrossRef]
58. Ghimire, U.; Bheemasetti, T.V.; Kim, H.-J. Performance of Stabilized Copper Mine Tailings with Freeze-Thaw and Wet-Dry Seasonal Cycles. *J. Rock Mech. Geotech. Eng.* **2025**, *17*, 1418–1428. [CrossRef]
59. Hwang, H.; Cho, B.; Choi, Y.C. Alkali Activation Mechanisms and Hydration Characteristics of Lithium Slag for Zero-Cement Binder Applications. *Case Stud. Constr. Mater.* **2026**, *24*, e06177. [CrossRef]

60. Zhao, Y.; Cui, C.; Gao, F.; Qi, Q.; Liu, Z.; Ma, X.; Jiang, X. Alkali–Silicate–Aluminate Synergistic Hydration Mechanisms for Enhanced Strength Development in High-Volume Lithium Slag Cement. *Clean. Mater.* **2026**, *19*, 100368. [CrossRef]
61. Santos, A.; Andrejkovičová, S.; Římnáčová, D.; Perná, I.; Almeida, F.; Rocha, F. Synthesis and Characterization of Lightweight Foamed Geopolymers from Iron Tailings for Energy-Efficient Construction. *J. Build. Eng.* **2026**, *120*, 115414. [CrossRef]
62. Sun, W.; Ma, B.; Tang, Y.; Li, X.; Li, X.; Zeng, Y.; Zou, Z. Mechanisms and Pore Properties of Eco-Friendly Alkali-Activated Foam Materials Prepared with Ilmenite Tailings and Metakaolin. *Case Stud. Constr. Mater.* **2025**, *23*, e05030. [CrossRef]
63. Li, J.; Liu, X.; Cai, C.; Li, F.; Jin, H.; Zhang, S.; Sheng, N.; Wang, T.; Ngo, T. Microstructure, Strength Development Mechanism and CO_2 Emission Assessments of Molybdenum Tailings Collaborative Fly Ash Geopolymers. *Case Stud. Constr. Mater.* **2024**, *21*, e03608. [CrossRef]
64. Bouchikhi, A.; Amar, M.; Arroug, L.; Safhi, A.E.M.; Haddaji, Y. Characterizing Nano-Indentation and Microstructural Properties of Mine Tailings-Based Geopolymers. *Case Stud. Constr. Mater.* **2024**, *21*, e03899. [CrossRef]
65. Niu, H.; Helser, J.; Corfe, I.J.; Kuva, J.; Butcher, A.R.; Cappuyns, V.; Kinnunen, P.; Illikainen, M. Incorporation of Bioleached Sulfidic Mine Tailings in One-Part Alkali-Activated Blast Furnace Slag Mortar. *Constr. Build. Mater.* **2022**, *333*, 127195. [CrossRef]
66. Liu, G.; Zhu, Y.; Wan, X.; Xu, P.; Wu, C.; Yu, H. Mechanical Properties of Alkali-Activated Red Mud Aggregate Concrete: Experimental Study and Mechanism Analysis. *Results Eng.* **2026**, *29*, 108694. [CrossRef]
67. Xie, G.; Suo, Y.; Liu, L.; Zhu, M.; Xie, L.; Qu, H.; Sun, W. Mechanical Grinding Activation of Modified Magnesium Slag and Its Use as Backfilling Cementitious Material. *Case Stud. Constr. Mater.* **2023**, *18*, e01778. [CrossRef]
68. Adediran, A.; Yliniemi, J.; Carvelli, V.; Adesanya, E.; Illikainen, M. Durability of Alkali-Activated Fe-Rich Fayalite Slag-Based Mortars Subjected to Different Environmental Conditions. *Cem. Concr. Res.* **2022**, *162*, 106984. [CrossRef]
69. Hou, S.; Guo, Y.; Sun, J.; Jiang, J.; Gao, H.; Liu, J. Prospect of Gold Tailings as a New Mineral Admixture: Effect on Hydration, Pore Structure and Mechanical Properties of Concrete. *Mater. Today Sustain.* **2025**, *29*, 101078. [CrossRef]
70. Sheik Farid, A.; Jayaseelan, R.; Pandulu, G. Novel Synthesis of Industrial and Agro Waste-Derived Non-Autoclaved Aerated Geopolymer Composites. *Next Mater.* **2026**, *11*, 101626. [CrossRef]
71. Wang, W.; Zhong, Z.; Kang, X.; Ma, X. Physico-Mechanical Properties and Micromorphological Characteristics of Graphene Oxide Reinforced Geopolymer Foam Concrete. *J. Build. Eng.* **2023**, *72*, 106732. [CrossRef]
72. Niu, H.; Abdulkareem, M.; Sreenivasan, H.; Kantola, A.M.; Havukainen, J.; Horttanainen, M.; Telkki, V.-V.; Kinnunen, P.; Illikainen, M. Recycling Mica and Carbonate-Rich Mine Tailings in Alkali-Activated Composites: A Synergy with Metakaolin. *Miner. Eng.* **2020**, *157*, 106535. [CrossRef]
73. Komnitsas, K.; Zaharaki, D.; Perdikatsis, V. Geopolymerisation of Low Calcium Ferronickel Slags. *J. Mater. Sci.* **2007**, *42*, 3073–3082. [CrossRef]
74. Van Deventer, J.S.J.; Provis, J.L.; Duxson, P.; Lukey, G.C. Reaction Mechanisms in the Geopolymeric Conversion of Inorganic Waste to Useful Products. *J. Hazard. Mater.* **2007**, *139*, 506–513. [CrossRef]
75. Lei, Z.; Zhao, L.; Zhong, F.; Huang, J. Sustainable All-Solid-Waste Ternary Geopolymer Grouting Materials: Mechanical Performance and Microstructural Evolution. *Dev. Built Environ.* **2026**, *25*, 100835. [CrossRef]
76. Chen, Y.; Wu, Z.; Zeng, C.; Liu, Y.; Pu, S.; Zhang, H.; Feng, Z.; Xu, K.; Ni, D. Study on the Workability, Strength, Durability and Environmental Performance of Alkali-Activated Electrolytic Manganese Slag-Fly Ash-Slag Grouting Materials. *Case Stud. Constr. Mater.* **2025**, *22*, e04199. [CrossRef]
77. Tang, R.; Zhao, B.-C.; Xin, J.; Sun, J.; Xu, B.; Tian, C.; Ning, J.; Li, L.; Shao, X.; Ren, W. Multisolid Waste Collaborative Production of Aeolian Sand-Red Mud-Fly Ash Cemented Paste Backfill. *Case Stud. Constr. Mater.* **2024**, *20*, e02843. [CrossRef]
78. Lang, L.; Zhu, M.; Pu, S. Recycling Engineering Sediment Waste as Sustainable Subgrade Material Using Ground Granulated Blast-Furnace Slag, Electrolytic Manganese Residue and Cement. *Environ. Technol. Innov.* **2025**, *37*, 103969. [CrossRef]
79. Li, K.; Li, X.; Yao, J.; Sun, Q.; Xue, H.; Du, C. Innovative Synthesis of Low-Carbon Cemented Backfill Materials through Synergistic Activation of Solid Wastes: An Integrated Assessment of Economic and Environmental Impacts. *Case Stud. Constr. Mater.* **2024**, *20*, e03203. [CrossRef]
80. Ding, Q.; Liu, L.; Wang, P.; Liu, W.; Li, J.; Zou, W. Durability and Erosion of Electrolytic Manganese Residues Modified by Low-Temperature Thermal Treatment for Karst Grouting Materials. *J. Rock Mech. Geotech. Eng.* **2026**, *18*, 6489–6505. [CrossRef]
81. Wang, Y.; Cheng, J.; Maimait, A.; Duan, Y.; Yang, L.; Chen, Q. Road Performance and Strength Mechanism of Aeolian Sand Subgrade Solidified by Full Solid-Waste Cementitious Materials. *Results Eng.* **2026**, *30*, 110541. [CrossRef]
82. Lv, Y.; Liu, Y.; Lan, J.; Zhang, T.C.; Li, J.; Liu, X.; Yao, J. Strength Optimization and Characterization of One-Part Geopolymer Prepared from Alkaline Thermo-Mechanical Activated Electrolytic Manganese Residue and Vanadium-Bearing Shale Leaching Residue. *Dev. Built Environ.* **2025**, *22*, 100660. [CrossRef]
83. Harmaji, A.; Jafari, R.; Simard, G. Durable Bauxite-Residue Geopolymers: Enhancing Scaling Resistance with Fly Ash and Waste Glass Powder. *Constr. Build. Mater.* **2025**, *491*, 142661. [CrossRef]
84. Gomes Silveira, N.C.; Figueiredo Martins, M.L.; Bezerra, A.C.D.S.; Gabriel Da Silva Araújo, F. Ecological Geopolymer Produced with a Ternary System of Red Mud, Glass Waste, and Portland Cement. *Clean. Eng. Technol.* **2022**, *6*, 100379. [CrossRef]

85. Yu, X.; Zhang, M.; Li, C.; Hayano, K.; Kang, X. Synergistic Effects of Recycled Demolition Waste and GGBS-FA Based Geopolymers on the Mechanical Properties and Stabilization Mechanism of High Plasticity Clay. *Case Stud. Constr. Mater.* **2024**, *20*, e03261. [CrossRef]
86. Zhao, G.; Yuan, X.; Yan, H.; Tian, J.; Wang, Y.; Xu, P.; Zhao, L.; Wang, W.; Liu, B. Resource Utilization of Waste Bored Pile Slurry: Properties, Mechanisms and Environmental Safety of Geopolymer-Based Lightweight Controlled Low-Strength Materials. *Constr. Build. Mater.* **2026**, *506*, 144864. [CrossRef]
87. Zhang, L.; Huang, B.; Zhao, X.; Yang, T.; Sun, C.; Zhao, M. Feasibility of Solid Waste-Based Geopolymers for Anti-Scouring Protection of Offshore Scour Pits: Macro-Performance, Micro-Characterization, and Sustainability. *Case Stud. Constr. Mater.* **2025**, *23*, e05583. [CrossRef]
88. Zhu, D.; Yan, C.; Liu, J.; Jia, Y.; Yin, Q.; Feng, G. A Study on Cemented Paste Backfill Using Red Mud and Coal Gasification Slag Based on Extreme Vertices Mixture Design. *Case Stud. Constr. Mater.* **2026**, *24*, e05853. [CrossRef]
89. Pang, H.; Huang, Y.; Qi, W.; Zhao, Q.; Wang, Y.; Zhao, D.; Kong, F.; Han, J. Preparation of Sustainable Backfill Cementitious Materials: Mix Proportion Optimization, Hydration Mechanism, and Sustainability Assessment. *Green Smart Min. Eng.* **2026**, *3*, 41–53. [CrossRef]
90. Cao, Y.; Mei, Y.; Yao, H.; Hu, B. Mechanical and Microstructural Characterization of One-Part Binder Incorporated with Alkali-Thermal Activated Red Mud. *Case Stud. Constr. Mater.* **2024**, *21*, e03634. [CrossRef]
91. Matalkah, F.; Soroushian, P. Shelf Life of Alkali Activated Cement: Effects of Storage Condition and Duration. *Constr. Build. Mater.* **2019**, *222*, 664–672. [CrossRef]
92. Rasuli, M.I.; Tajunnisa, Y.; Yamamura, A.; Shigeishi, M. A Consideration on the One-Part Mixing Method of Alkali-Activated Material: Problems of Sodium Silicate Solubility and Quick Setting. *Heliyon* **2022**, *8*, e08783. [CrossRef]
93. Almakhadmeh, M.; Soliman, A.M. Effects of Mixing Water Temperatures on Properties of One-Part Alkali-Activated Slag Paste. *Constr. Build. Mater.* **2021**, *266*, 121030. [CrossRef]
94. Chen, Z.; Liu, Y.; Li, Y.; Li, K.; Zhang, C.; Kang, X. Performance Improvement and Mechanism of Steel Slag Geopolymers Modified with Recycled Wind Turbine Blade Powders. *Sustain. Mater. Technol.* **2026**, *48*, e02009. [CrossRef]
95. Saputra, A.A.I.; Soemitro, R.A.A.; Satrya, T.R.; Warnana, D.D.; Muntaha, M.; Maulana, M.A.; Zerfu, K.; Zewdie, E.A.; Laory, I.; Ekaputri, J.J. Hydraulic Conductivity of CFBC Fly Ash-Based Geopolymer: Toward Sustainable Liner Materials. *Green Technol. Sustain.* **2026**, *4*, 100325. [CrossRef]
96. Hu, Z.; Ma, Q.; Lu, H.; Xu, X.; Zhao, G.; Jiang, N. Synergistic High-Dosage Phosphogypsum and Multi-Solid Wastes in Subgrade Fillers: Mechanical Properties, Micro-Mechanisms, and Environmental Compliance. *J. Rock Mech. Geotech. Eng.* **2026**, *18*, 4796–4811. [CrossRef]
97. Wan, Q.; Rao, F.; Song, S.; Morales-Estrella, R.; Xie, X.; Tong, X. Chemical Forms of Lead Immobilization in Alkali-Activated Binders Based on Mine Tailings. *Cem. Concr. Compos.* **2018**, *92*, 198–204. [CrossRef]
98. Wan, Q.; Rao, F.; Song, S.; Zhang, Y. Immobilization Forms of ZnO in the Solidification/Stabilization (S/S) of a Zinc Mine Tailing through Geopolymerization. *J. Mater. Res. Technol.* **2019**, *8*, 5728–5735. [CrossRef]
99. Farias Castillo, I.; Aponte, D.; Barra, M. Leaching Behavior and Alkali Activation Potential of Copper and Black Slags: Compliance and pH-Dependence Test, and Development of Alkali-Activated Pastes. *Case Stud. Constr. Mater.* **2025**, *23*, e05562. [CrossRef]
100. Wijesekara, K.K.D.A.; Sadique, M.; Carnacina, I.; De Sande, V.T.; Al-Hasani, B. Performance Evaluation of Recycled Aggregate Geopolymer Concrete for Low-Carbon Breakwater Systems. *Clean. Waste Syst.* **2026**, *13*, 100455. [CrossRef]
101. Hoy, M.; Horpibulsuk, S.; Rachan, R.; Chinkulkijniwat, A.; Arulrajah, A. Recycled Asphalt Pavement–Fly Ash Geopolymers as a Sustainable Pavement Base Material: Strength and Toxic Leaching Investigations. *Sci. Total Environ.* **2016**, *573*, 19–26. [CrossRef]
102. Ji, X.; Chen, B.; Dong, X.; Lu, H.; Zhang, X.; He, S.; Wu, T. Mechanical and Environmental Properties of Geopolymer-Stabilized Domestic Waste Incineration Slag in an Asphalt Pavement Base. *J. Road Eng.* **2023**, *3*, 218–228. [CrossRef]
103. Al Noman, A.; Islam, M.R.; Khan, M.Z.A.; Islam, M.R.; Islam, K.A.; Ahmed, T. High-Strength and Low-Absorption Geopolymer Artificial Aggregates Produced under Heat, Autoclave, and Heat-Solution Curing. *Case Stud. Constr. Mater.* **2025**, *23*, e05222. [CrossRef]
104. Lu, X.; Tian, Y.; Jiskani, I.M.; Zhou, W.; Zhao, B.; Ding, X.; Ao, Z. Innovate Geopolymer Synthesis for Green Mine Road Construction: Analysis of Efflorescence Behavior and Strength Analysis. *Constr. Build. Mater.* **2023**, *401*, 132963. [CrossRef]
105. Qin, Z.; Yuan, Y.; Chen, Z.; Li, Y.; Xia, Y. Combined Preparation and Application of Geopolymer Pavement Materials from Coal Slurry-Slag Powder-Fly Ash Mining Solid Waste: A Case Study. *Constr. Build. Mater.* **2024**, *441*, 137510. [CrossRef]
106. Kriskova, L.; Ducman, V.; Loncnar, M.; Tesovnik, A.; Žibret, G.; Skentzou, D.; Georgopoulos, C. Alkali-Activated Mineral Residues in Construction: Case Studies on Bauxite Residue and Steel Slag Pavement Tiles. *Materials* **2025**, *18*, 257. [CrossRef]
107. Mahmood, A.H.; Zahid, C.Z.B.; Foster, S.J. High-density Geopolymer Concrete Exposed to Marine Environment. *Struct. Concr.* **2025**, *26*, 5282–5285. [CrossRef]
108. Nazari, A.; Pacheco Torgal, F. Predicting Compressive Strength of Different Geopolymers by Artificial Neural Networks. *Ceram. Int.* **2013**, *39*, 2247–2257. [CrossRef]

109. Nazari, A.; Sanjayan, J.G. Modelling of Compressive Strength of Geopolymer Paste, Mortar and Concrete by Optimized Support Vector Machine. *Ceram. Int.* **2015**, *41*, 12164–12177. [CrossRef]
110. Nguyen, K.T.; Nguyen, Q.D.; Le, T.A.; Shin, J.; Lee, K. Analyzing the Compressive Strength of Green Fly Ash Based Geopolymer Concrete Using Experiment and Machine Learning Approaches. *Constr. Build. Mater.* **2020**, *247*, 118581. [CrossRef]
111. Cao, R.; Fang, Z.; Jin, M.; Shang, Y. Application of Machine Learning Approaches to Predict the Strength Property of Geopolymer Concrete. *Materials* **2022**, *15*, 2400. [CrossRef]
112. Peng, Y.; Unluer, C. Analyzing the Mechanical Performance of Fly Ash-Based Geopolymer Concrete with Different Machine Learning Techniques. *Constr. Build. Mater.* **2022**, *316*, 125785. [CrossRef]
113. Ghosh, A.; Ransinchung, G.D. Application of Machine Learning Algorithm to Assess the Efficacy of Varying Industrial Wastes and Curing Methods on Strength Development of Geopolymer Concrete. *Constr. Build. Mater.* **2022**, *341*, 127828. [CrossRef]
114. Shen, J.; Li, Y.; Lin, H.; Li, H.; Lv, J.; Feng, S.; Ci, J. Prediction of Compressive Strength of Alkali-Activated Construction Demolition Waste Geopolymers Using Ensemble Machine Learning. *Constr. Build. Mater.* **2022**, *360*, 129600. [CrossRef]
115. Hsu, C.-H.; Chan, H.-Y.; Chang, M.-H.; Liu, C.-F.; Liu, T.-Y.; Chiu, K.-C. Efficient Compressive Strength Prediction of Alkali-Activated Waste Materials Using Machine Learning. *Materials* **2024**, *17*, 3141. [CrossRef]
116. Zhang, L.V.; Marani, A.; Nehdi, M.L. Chemistry-Informed Machine Learning Prediction of Compressive Strength for Alkali-Activated Materials. *Constr. Build. Mater.* **2022**, *316*, 126103. [CrossRef]
117. Ke, X.; Duan, Y. Coupling Machine Learning with Thermodynamic Modelling to Develop a Composition-Property Model for Alkali-Activated Materials. *Compos. Part B Eng.* **2021**, *216*, 108801. [CrossRef]
118. Ding, Y.; Wei, W.; Wang, J.; Wang, Y.; Shi, Y.; Mei, Z. Prediction of Compressive Strength and Feature Importance Analysis of Solid Waste Alkali-Activated Cementitious Materials Based on Machine Learning. *Constr. Build. Mater.* **2023**, *407*, 133545. [CrossRef]
119. Shah, S.F.A.; Chen, B.; Zahid, M.; Ahmad, M.R. Compressive Strength Prediction of One-Part Alkali Activated Material Enabled by Interpretable Machine Learning. *Constr. Build. Mater.* **2022**, *360*, 129534. [CrossRef]
120. Nazar, S.; Yang, J.; Amin, M.N.; Khan, K.; Ashraf, M.; Aslam, F.; Javed, M.F.; Eldin, S.M. Machine Learning Interpretable-Prediction Models to Evaluate the Slump and Strength of Fly Ash-Based Geopolymer. *J. Mater. Res. Technol.* **2023**, *24*, 100–124. [CrossRef]
121. Sun, Y.; Cheng, H.; Zhang, S.; Mohan, M.K.; Ye, G.; De Schutter, G. Prediction & Optimization of Alkali-Activated Concrete Based on the Random Forest Machine Learning Algorithm. *Constr. Build. Mater.* **2023**, *385*, 131519. [CrossRef]
122. Li, Y.; Shen, J.; Lin, H.; Li, Y. Optimization Design for Alkali-Activated Slag-Fly Ash Geopolymer Concrete Based on Artificial Intelligence Considering Compressive Strength, Cost, and Carbon Emission. *J. Build. Eng.* **2023**, *75*, 106929. [CrossRef]
123. Dong, W.; Huang, Y.; Cui, A.; Ma, G. Mix Design Optimization for Fly Ash-Based Geopolymer with Mechanical, Environmental, and Economic Objectives Using Soft Computing Technology. *J. Build. Eng.* **2023**, *72*, 106577. [CrossRef]
124. Ji, H.; Lyu, Y.; Ying, W.; Liu, J.-C.; Ye, H. Machine Learning Guided Iterative Mix Design of Geopolymer Concrete. *J. Build. Eng.* **2024**, *91*, 109710. [CrossRef]
125. Kazemi, F.; Shafighfard, T.; Jankowski, R.; Yoo, D.-Y. Active Learning on Stacked Machine Learning Techniques for Predicting Compressive Strength of Alkali-Activated Ultra-High-Performance Concrete. *Arch. Civ. Mech. Eng.* **2024**, *25*, 24. [CrossRef]
126. Zhong, W.L.; Ding, H.; Zhao, X.; Fan, L.F. Mechanical Properties Prediction of Geopolymer Concrete Subjected to High Temperature by BP Neural Network. *Constr. Build. Mater.* **2023**, *409*, 133780. [CrossRef]
127. Yao, C.; Hu, G.; Chen, Q.; Wu, J. Prediction on the Freeze-Thaw Resistance of a One-Part Geopolymer Stabilized Soil by Using Deep Learning Method. *Case Stud. Constr. Mater.* **2024**, *21*, e03530. [CrossRef]
128. Bian, Y.; Xiang, W.; Zhang, Q.; Wu, T.; Wang, J.; Hui, D. Upcycled Geopolymer Concrete Incorporating GFRP Waste Powder: Sulfate Resistance and Machine Learning-Based Strength Prediction. *Dev. Built Environ.* **2026**, *26*, 100900. [CrossRef]
129. Pei, J.S.F.; Choo, C.S.; Khaerudini, D.S.; Bong, S.H.; Ong, D.E.L.; Sunarso, J. Evaluation of Strength Development of One-Part Alkali-Activated Materials through Machine Learning and Thermodynamic Modelling. *Cem. Concr. Compos.* **2026**, *165*, 106364. [CrossRef]
130. Zheng, S.; Liu, Z.; Huang, J.; Liu, L.; Jin, Q.; Zhang, Q.; Liu, Z.; Tang, G. A Review of Machine Learning Methods for Geopolymer Performance Prediction: Linking Data-Driven Models with Physical Insights. *J. Build. Eng.* **2025**, *114*, 114227. [CrossRef]

Disclaimer/Publisher's Note: The statements, opinions and data contained in all publications are solely those of the individual author(s) and contributor(s) and not of MDPI and/or the editor(s). MDPI and/or the editor(s) disclaim responsibility for any injury to people or property resulting from any ideas, methods, instructions or products referred to in the content.